

An analysis of implicit time integration schemes for wave propagations

Sun-Beom Kwon^a, Klaus-Jürgen Bathe^b, Gunwoo Noh^{c,*}

^a Hyundai Heavy Industries, Ulsan 44032, Republic of Korea

^b Massachusetts Institute of Technology, Cambridge, MA 02139, USA

^c Kyungpook National University, Daegu 41566, Republic of Korea

ARTICLE INFO

Article history:

Received 18 October 2019

Accepted 12 December 2019

Keywords:

Wave propagations

Finite elements

Direct time integrations

Implicit schemes

Trapezoidal rule, Newmark and Bathe methods

Numerical dispersion

ABSTRACT

The objective of this paper is to investigate the optimal use of some time integration schemes for the solution of transient wave propagation problems. We study the accuracy characteristics of the trapezoidal rule and the ρ_∞ -Bathe scheme considering various parameter sets (ρ_∞, γ, CFL) with both consistent and lumped mass matrices. The ρ_∞ -Bathe scheme includes also the standard-, β_1/β_2 -Bathe methods, the Newmark method and the trapezoidal rule. The study of the numerical dispersion shows that in the case of the consistent mass matrix, the ρ_∞ -Bathe scheme with a proper setting of (ρ_∞, γ) and standard Bathe scheme provide similar dispersion errors and outperform the trapezoidal rule. The optimal CFL number of the ρ_∞ -Bathe scheme is about 25% larger than for the standard Bathe scheme. In addition, we show that using a lumped mass matrix and proper values of $\rho_\infty < 0, \gamma$ and CFL in the ρ_∞ -Bathe scheme, more accurate solutions can be obtained in some analyses.

© 2019 Elsevier Ltd. All rights reserved.

1. Introduction

The finite element method with direct time integration is widely used to solve structural dynamics and transient wave propagation problems in solids [1–3]. Direct time integrations can be classified into implicit and explicit schemes [3]. Implicit methods are frequently treated as the first-line strategy in practical use due to their unconditional stability, while explicit schemes can also be effective for some analyses of short-duration events, e.g., impact, crash, or short-duration wave propagations.

We focus in this paper on implicit schemes. Much research effort has been focused on developing enhanced implicit time integration methods and identifying their effective uses [4–16]. Among different strategies, a composite strategy with sub-steps is increasingly proposed [17–24]. The first implicit composite scheme for structural dynamics, referred to here as the “standard” Bathe implicit time integration method [25,26], has attracted much attention due to the characteristic of suppressing efficiently high-frequency inaccurate modes while retaining good accuracy in the important low-frequency modes [27–29]. The composite strategy with a sub-step was also adopted in the development of explicit methods for structural dynamics and wave propagations [30–33].

The standard Bathe method is a two sub-step method in which a trapezoidal rule and Euler three-point backward formula are

used in the first and second sub-steps, respectively. An important extension of the standard Bathe scheme was proposed by Noh and Bathe, the ρ_∞ -Bathe scheme [34]. This method contains the Newmark method, the trapezoidal rule, as well as the standard and β_1/β_2 -Bathe schemes [35,36].

Direct time integration is widely used for the solution of wave propagation problems. Accurate solutions are difficult to obtain due to numerical errors of dispersion and dissipation arising from the spatial and temporal approximations [37–39]. For this reason, enhanced spatial approximations are considered [40–44]. If for the direct time integration an implicit scheme is used, numerical dissipation to filter out highly inaccurate frequencies in the finite element model is usually necessary. The aim is to suppress the high frequencies and corresponding modes in the finite element model that are highly inaccurate compared to the actual continuum frequencies. Noh et al. and Kim et al. studied the dispersion properties of the standard Bathe method using for the spatial discretization the bilinear finite element and two enhancements, the method of finite spheres and overlapping finite elements [45,46,47]. The Bathe method used with the enhanced spatial approximations showed monotonic convergence of calculated solutions with decreasing time step size and a solution accuracy that is almost independent of the wave propagation directions through the mesh.

In the present study, our objective is to focus once again on the solution accuracy with standard displacement-based spatial discretizations, as in ref. [45], using regular meshes and implicit time integration. However, we now consider the specific parameters

* Corresponding author.

E-mail address: gunwoo@knu.ac.kr (G. Noh).

Table 1
Some important use of parameters in the ρ_∞ -Bathe time integration scheme in linear analyses. The scheme is in all cases here considered unconditionally stable and second-order accurate.

For structural vibrations:

- (1) Use ρ_∞ as input with γ optimal, i.e. $\gamma = \gamma_0$ given in Eq. (16)
- (2) Use $\rho_\infty = 0$ for general structures, but sometimes for structures with no stiff parts use $\rho_\infty = 1$; hardly use the values in-between, $\rho_\infty \in (0, 1)$; the ρ_∞ -Bathe method with $\rho_\infty = 0$ reduces to the standard Bathe scheme

For wave propagation problems (with linear finite elements):

- (1) Use consistent mass matrix, but sometimes use of the lumped mass matrix can be effective for problems where large numerical dissipation is needed.
- (2) With consistent mass matrix, use $\rho_\infty = 0, \gamma = \gamma_0, CFL = 1.0$, or use $\rho_\infty = 0.65, \gamma = \gamma_0, CFL = 1.25$ for similar accuracy with less computations.
- (3) With lumped mass matrix, use $\rho_\infty = 1 - \sqrt{3}, \gamma = 1.3$ and $CFL = 1.5$.

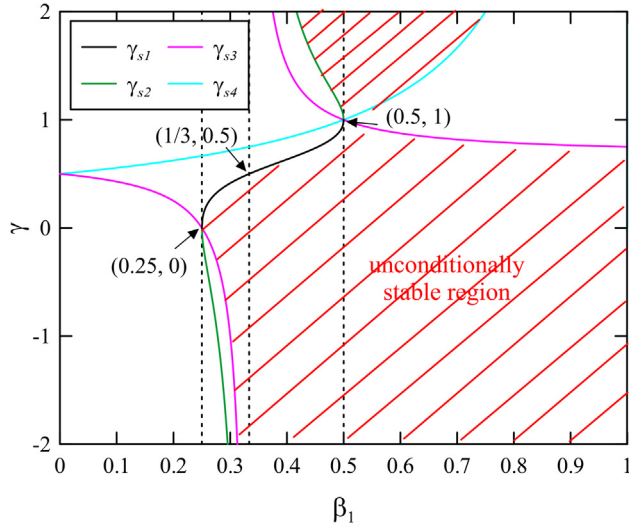


Fig. 1. Stability limit line of the β_1/β_2 -Bathe scheme with $\beta_2 = 2\beta_1$ for various values of β_1 .

used in the time integration schemes, CFL numbers, and the kind of mass matrix used. We want to identify the optimal use of the integration schemes when employed in simple regular standard finite element discretizations with consistent and lumped mass matrices. The results will be of general value and such regular spatial discretizations are also used in the AMORE scheme, in the interior of the analysis geometry [48,49]. First, in Section 2, we study the dispersion characteristics theoretically. Thereafter, we illustrate in Section 3 our findings in the predicted response solutions of one- (1D) and two-dimensional (2D) wave propagation problems.

2. Dispersion analyses

In this section, we analyze the dispersion errors of the trapezoidal rule and the ρ_∞ -Bathe methods for 1D and 2D wave propagation problems that we obtain with standard displacement-based spatial discretizations. For the 1D and 2D cases we use uniform meshes of the 2-node and 4-node elements, respectively. In the 1D case, we consider a mesh with nodes equally spaced Δx apart along the x axis ($\Delta x = h$, where h is the size of the element). In

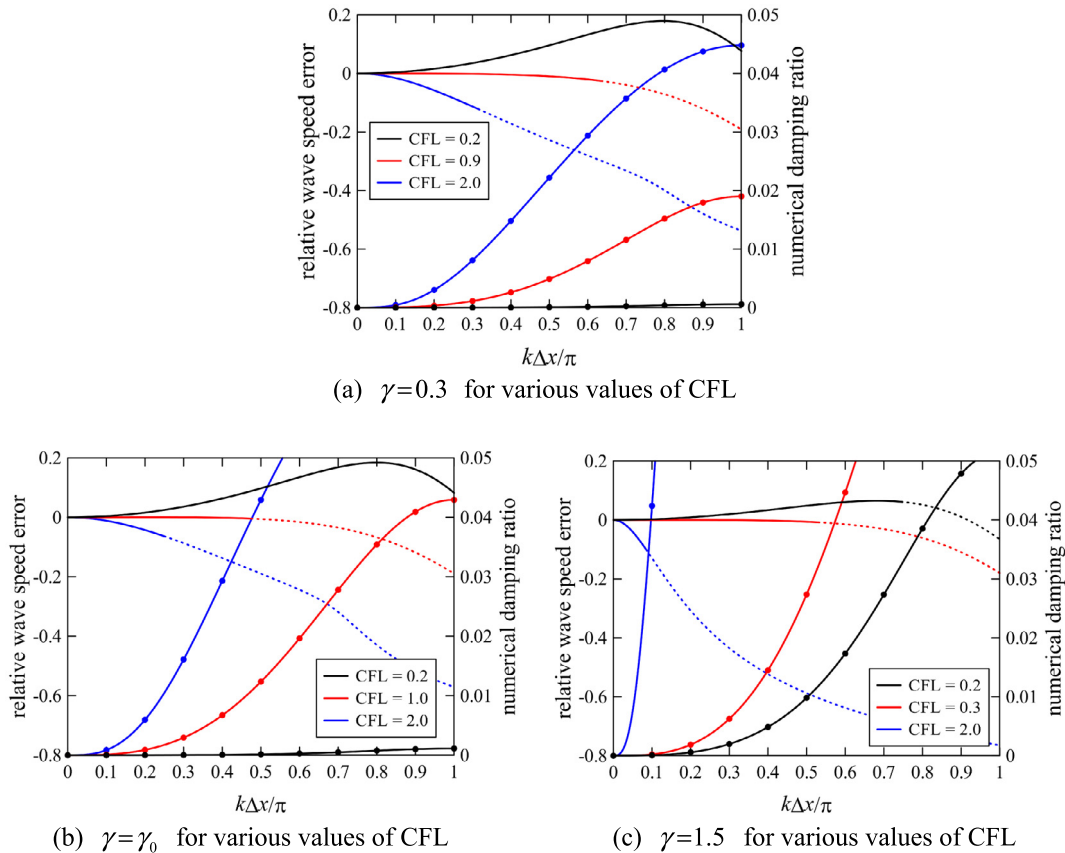


Fig. 2. Relative wave speed errors (left axis) and numerical damping ratio (right axis) of the ρ_∞ -Bathe scheme with the consistent mass matrix when $\rho_\infty = 0$ for various values of $\gamma > 0$ and CFL; results for solid and dotted lines are relative wave speed errors (dotted lines: discarded wave modes); and results for marked lines are the numerical damping ratio.

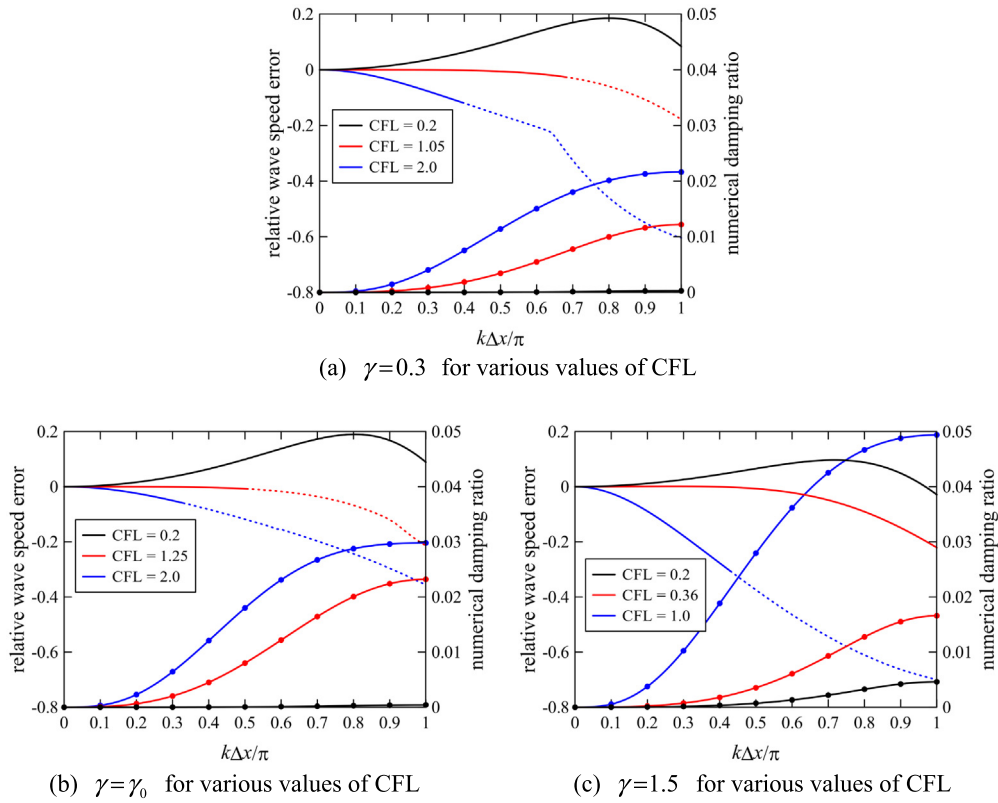


Fig. 3. Relative wave speed errors (left axis) and numerical damping ratio (right axis) of the ρ_∞ -Bathe scheme with the consistent mass matrix when $\rho_\infty = 0.65$ for various values of $\gamma > 0$ and CFL; results for solid and dotted lines are relative wave speed errors (dotted lines: discarded wave modes); and results for marked lines are the numerical damping ratio.

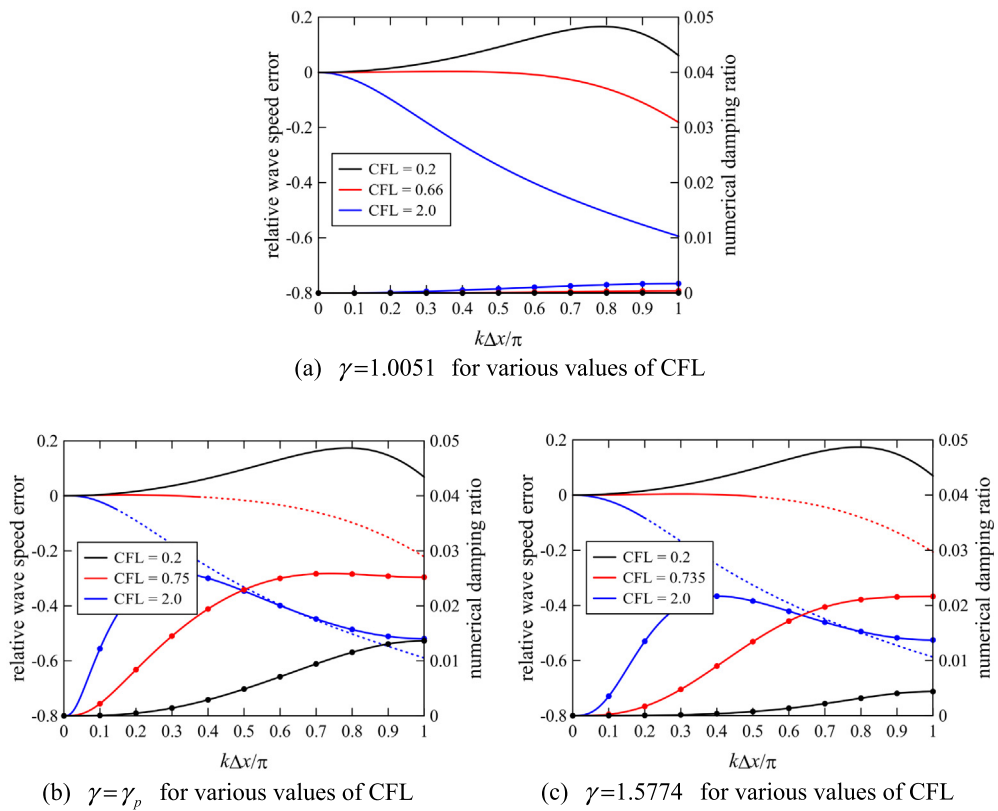


Fig. 4. Relative wave speed errors (left axis) and numerical damping ratio (right axis) of the ρ_∞ -Bathe scheme with the consistent mass matrix when $\rho_\infty = -0.9$ for various values of $\gamma > 1$ and CFL; results for solid and dotted lines are relative wave speed errors (dotted lines: discarded wave modes); and results for marked lines are the numerical damping ratio.

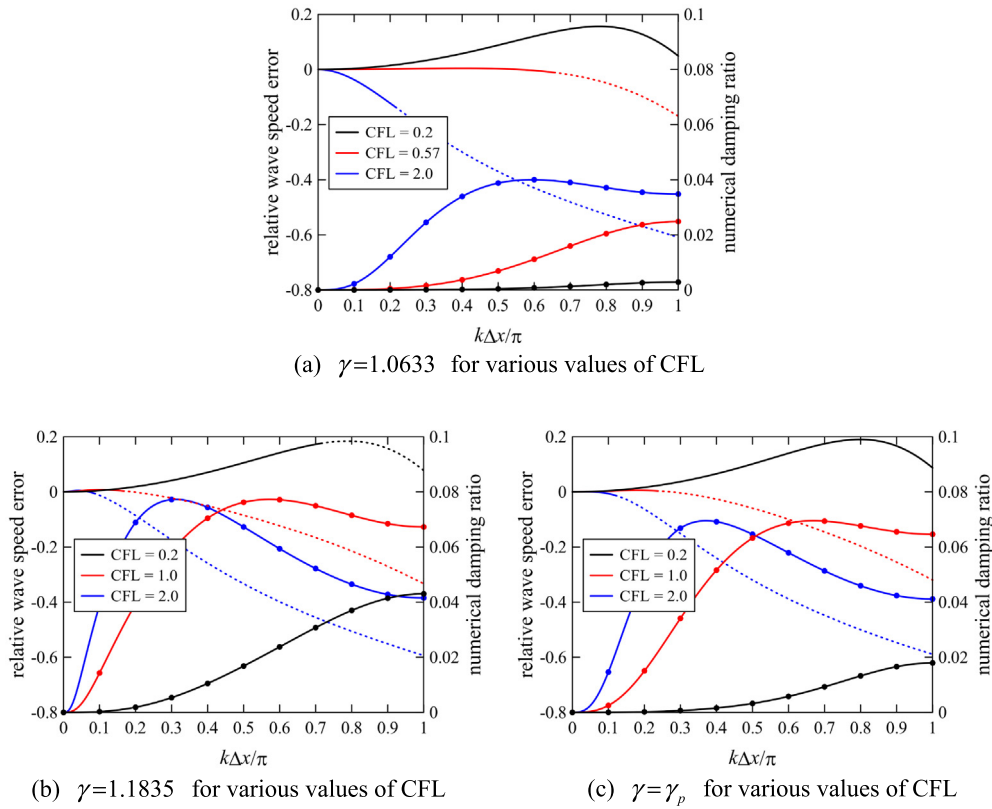


Fig. 5. Relative wave speed errors (left axis) and numerical damping ratio (right axis) of the ρ_∞ -Bathe scheme with the consistent mass matrix when $\rho_\infty = 1 - \sqrt{3}$ for various values of $\gamma > 1$ and CFL; results for solid and dotted lines are relative wave speed errors (dotted lines: discarded wave modes); and results for marked lines are the numerical damping ratio.

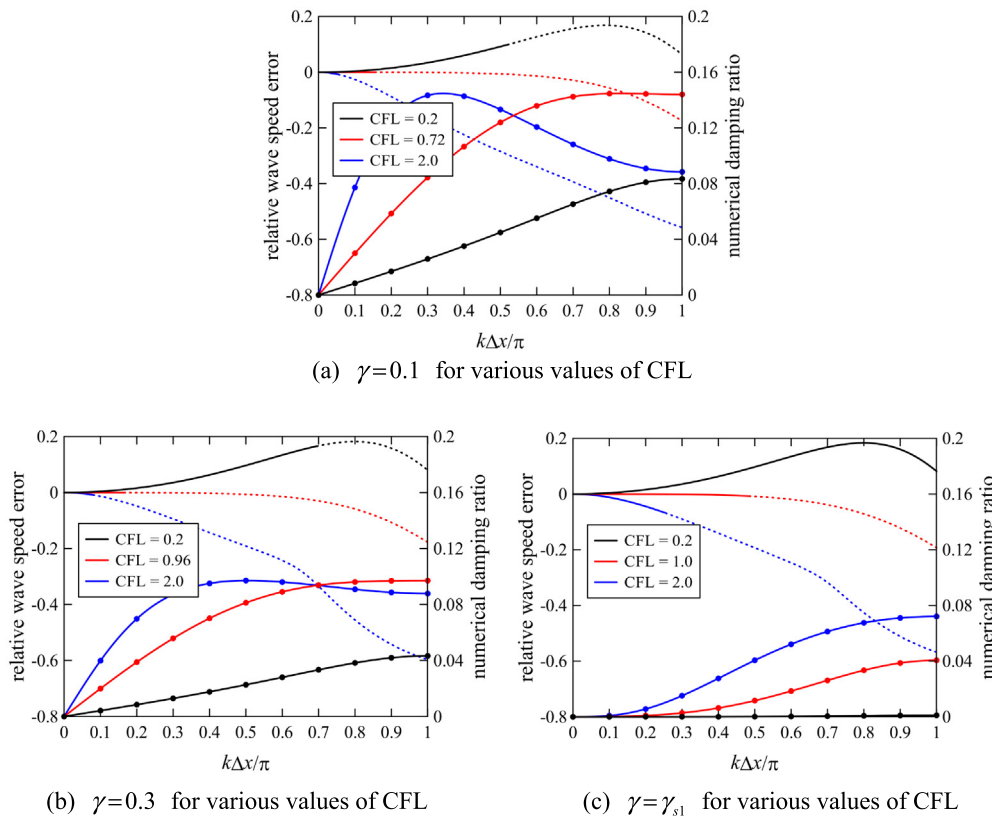


Fig. 6. Relative wave speed errors (left axis) and numerical damping ratio (right axis) of the β_1/β_2 -Bathe scheme with the consistent mass matrix when $\beta_1 = 1/3$ and $\beta_2 = 2\beta_1$ for various values of γ and CFL; results for solid and dotted lines are relative wave speed errors (dotted lines: discarded wave modes); and results for marked lines are the numerical damping ratio.

the 2D case, we use a mesh with element side lengths h ($\Delta x = h, \Delta y = h$) aligned with the (x, y) coordinate axes.

We consider the solution of the scalar wave governed by

$$\ddot{u} - c_0^2 \Delta u = 0 \tag{1}$$

where u , c_0 , and Δ are the field variable, exact wave velocity, and Laplace operator, and the over-dot denotes a time derivative. The corresponding solution is given by

$$u = A e^{i(k_0 \mathbf{n} \cdot \mathbf{y} - \omega_0 t)} \tag{2}$$

where A , k_0 , ω_0 and t are the amplitude, exact wave number, exact angular frequency, and time, respectively, and \mathbf{n} and \mathbf{y} are the unit vector in the direction of the wave propagation and the position vector, respectively, and i is the unit imaginary number. Note that the exact solution to Eq. (2) is non-dispersive, i.e. $c_0 = \omega_0/k_0$.

In the numerical solutions of Eq. (1), we have the wave speed error $c - c_0$, where c is the numerical wave speed. Since the wave speed error is a function of the wave number (or angular frequency) we have “numerical dispersion” in the solutions.

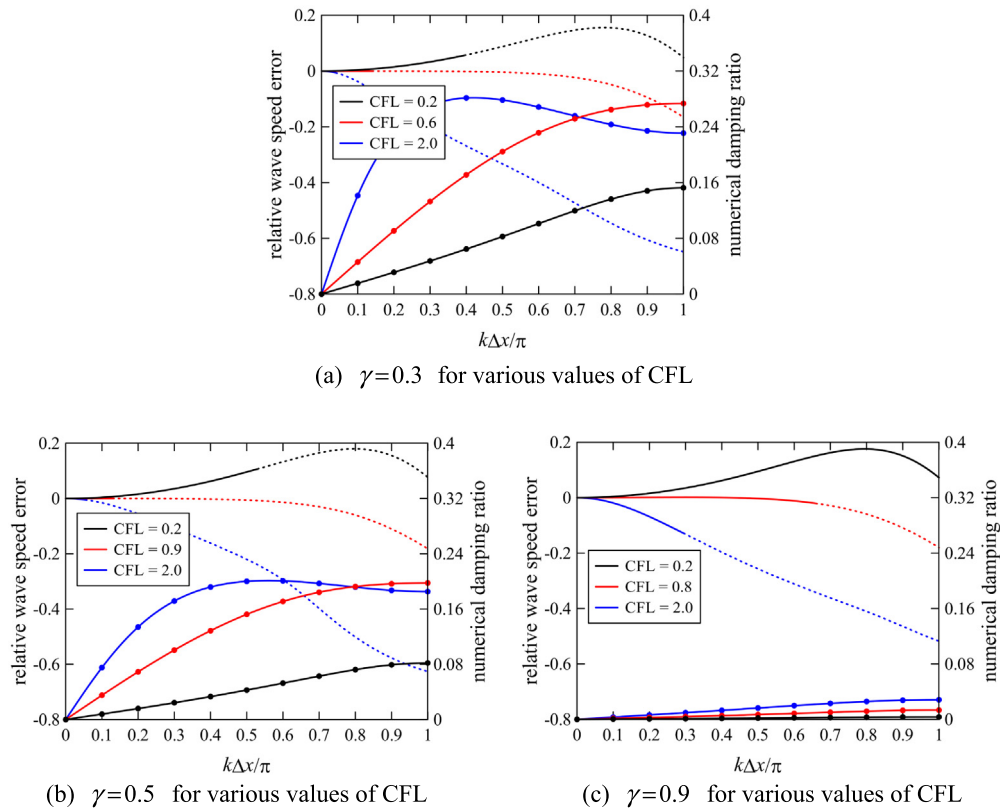


Fig. 7. Relative wave speed errors (left axis) and numerical damping ratio (right axis) of the β_1/β_2 -Bathe scheme with the consistent mass matrix when $\beta_1 = 0.5$ and $\beta_2 = 2\beta_1$ for various values of γ and CFL; results for solid and dotted lines are relative wave speed errors (dotted lines: discarded wave modes); and results for marked lines are the numerical damping ratio.

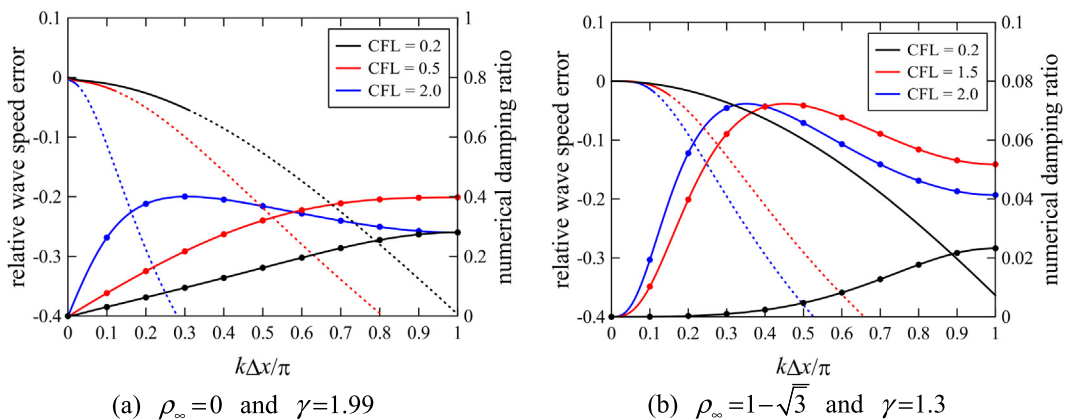


Fig. 8. Relative wave speed errors (left axis) and numerical damping ratio (right axis) of the ρ_∞ -Bathe scheme with the lumped mass matrix for various values of CFL; results for solid and dotted lines are relative wave speed errors (dotted lines: discarded wave modes); and results for marked lines are the numerical damping ratio.

To evaluate the dispersion error, we perform the analysis using the approaches of Refs. [45–47] but we modify the analysis procedure to ease the calculations. The analysis approaches used in Refs. [45–47] and in the present study are in essence only different in the order of calculations; therefore, all provide identical results.

We first evaluate the dispersion error that originates from the spatial approximation by considering the time-independent form of the wave equation

$$\Delta u + k_0^2 u = 0 \tag{3}$$

and the associated finite element discretization

$$\mathbf{K}\mathbf{U} - (k_0 h)^2 \mathbf{M}\mathbf{U} = \mathbf{0} \tag{4}$$

where \mathbf{U} , \mathbf{M} , and \mathbf{K} are the vector of unknown coefficients, the associated dimensionless mass and stiffness matrices.

We assume that the solution to Eq. (4) associated with node I , \mathbf{U}_I , to be the numerical sinusoidal plane waveform as

$$\mathbf{U}_I = \hat{\mathbf{U}} e^{ik\mathbf{n}\cdot\mathbf{y}_I} \tag{5}$$

where $\hat{\mathbf{U}}$ and \mathbf{y}_I are the amplitude and the position vector, and k is the solution wave number.

Substituting from Eq. (5) into Eq. (4), we obtain the finite element equations for all nodes

$$(\mathbf{D}_{\text{stiff}} - (k_0 h)^2 \mathbf{D}_{\text{mass}}) \hat{\mathbf{U}} = \mathbf{0} \tag{6}$$

where the entries in the matrices \mathbf{D}_{mass} and $\mathbf{D}_{\text{stiff}}$ are a function of k . We thus obtain a relationship between k_0 and k from the condition for existence of a nontrivial solution to Eq. (6)

$$\det(\mathbf{D}_{\text{stiff}} - (k_0 h)^2 \mathbf{D}_{\text{mass}}) = 0 \tag{7}$$

Next, to investigate the error from the time integration, we consider the scalar wave equation by substituting Eq. (2) into Eq. (1)

$$\ddot{u} + k_0^2 c_0^2 u = 0 \tag{8}$$

and focus on the effect of the time integration scheme. The total error is then obtained by accounting for the errors from the time and spatial discretizations (for the spatial interpolation using the relationship between k and k_0 obtained through Eq. (7)).

Since the general relations of the ρ_∞ -Bathe time integration scheme contain the Newmark method, trapezoidal rule and the β_1/β_2 -Bathe scheme [34], we focus here on using the ρ_∞ -Bathe equations

$${}^{t+\gamma\Delta t}\mathbf{U} = {}^t\mathbf{U} + \frac{\gamma\Delta t}{2} ({}^t\dot{\mathbf{U}} + {}^{t+\gamma\Delta t}\dot{\mathbf{U}}) \tag{9}$$

$${}^{t+\gamma\Delta t}\dot{\mathbf{U}} = {}^t\dot{\mathbf{U}} + \frac{\gamma\Delta t}{2} ({}^t\ddot{\mathbf{U}} + {}^{t+\gamma\Delta t}\ddot{\mathbf{U}}) \tag{10}$$

$${}^{t+\gamma\Delta t}\mathbf{U} = {}^t\mathbf{U} + \Delta t (q_0 {}^t\ddot{\mathbf{U}} + q_1 {}^{t+\gamma\Delta t}\ddot{\mathbf{U}} + q_2 {}^{t+\gamma\Delta t}\dot{\mathbf{U}}) \tag{11}$$

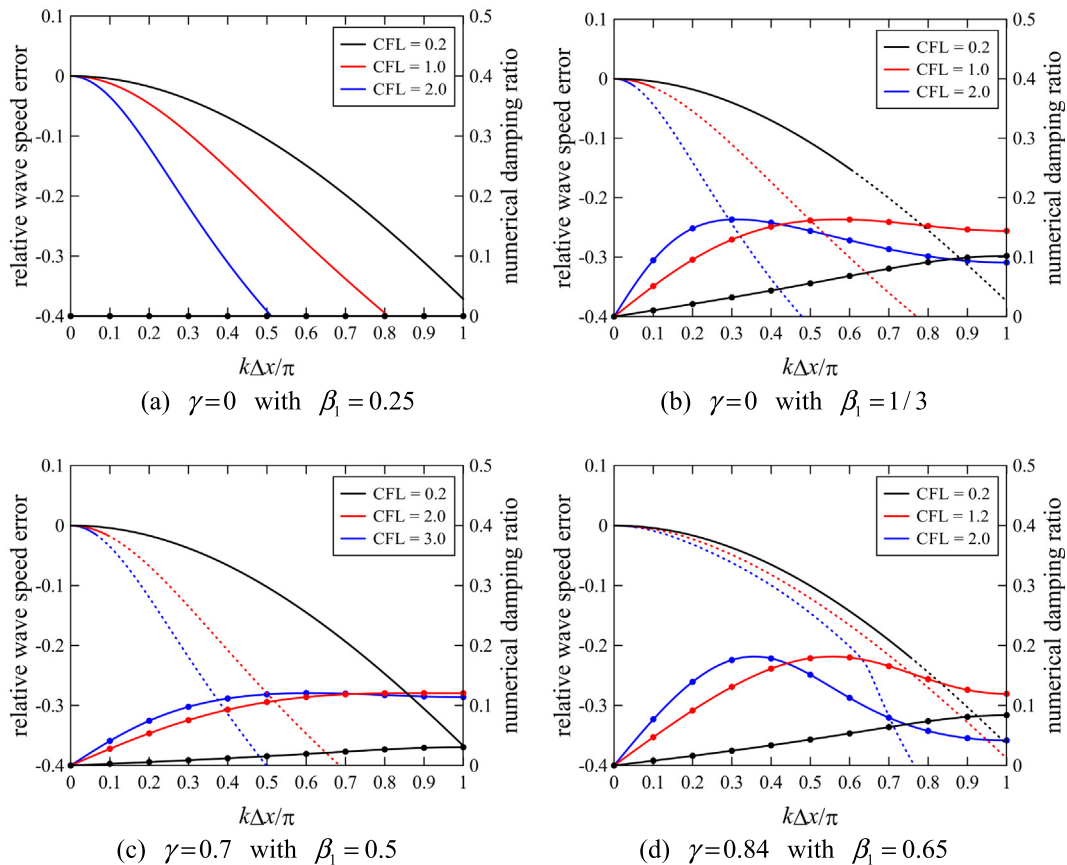


Fig. 9. Relative wave speed errors (left axis) and numerical damping ratio (right axis) of the β_1/β_2 -Bathe scheme ($\beta_2 = 2\beta_1$) with the lumped mass matrix for various values of CFL; results for solid and dotted lines are relative wave speed errors (dotted lines: discarded wave modes); and results for marked lines are the numerical damping ratio.

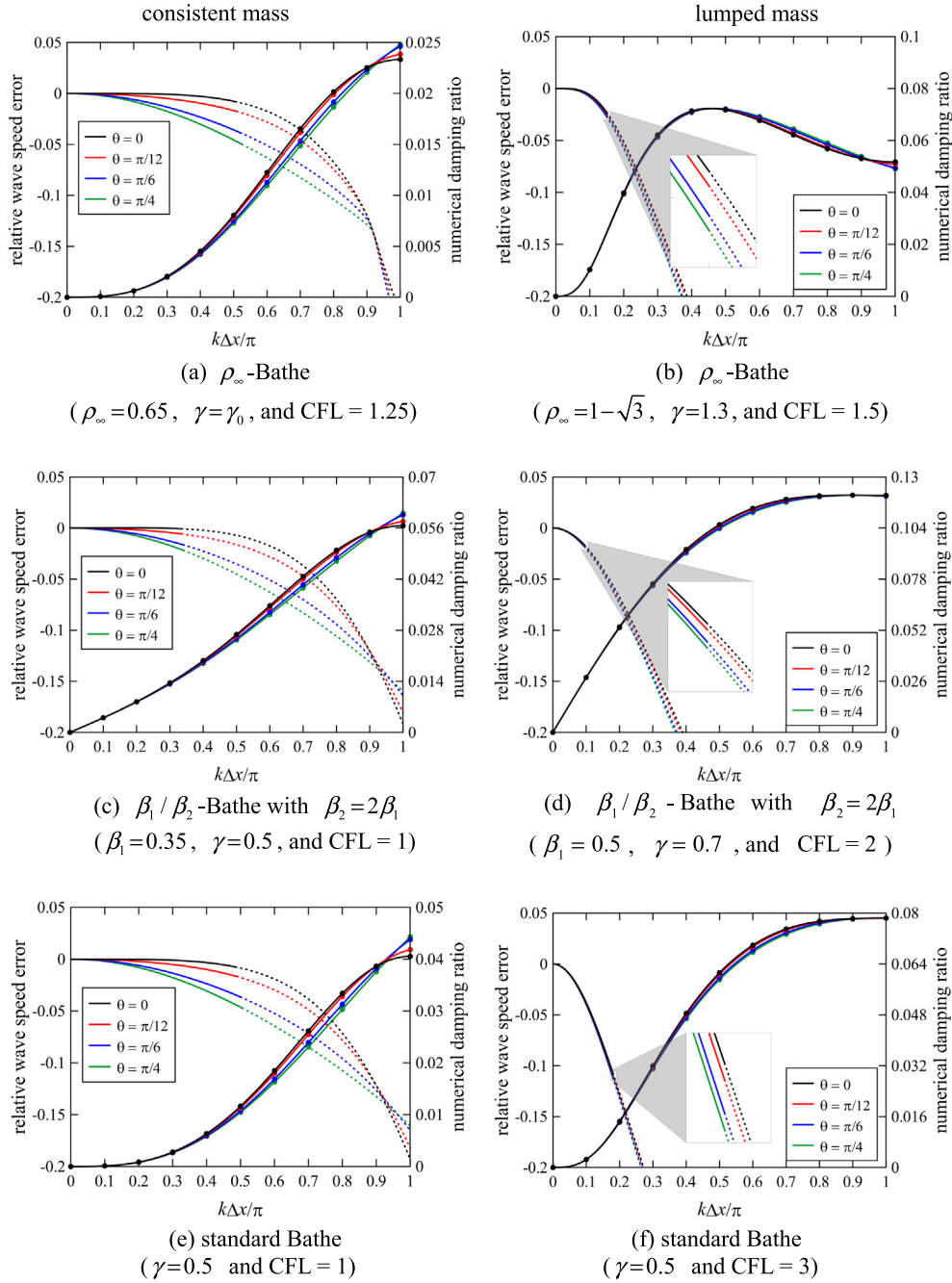


Fig. 10. Relative wave speed errors (left axis) and numerical damping ratio (right axis) of the Bathe schemes for various angles between wave propagation direction and the x axis; results for solid and dotted lines are relative wave speed errors (dotted lines: discarded wave modes); and results for marked lines are the numerical damping ratio.

$${}^{t+\gamma\Delta t}\dot{\mathbf{U}} = {}^t\dot{\mathbf{U}} + \Delta t \left(s_0 {}^t\ddot{\mathbf{U}} + s_1 {}^{t+\gamma\Delta t}\ddot{\mathbf{U}} + s_2 {}^{t+\gamma\Delta t}\ddot{\mathbf{U}} \right) \quad (12)$$

where $q_0, q_1, q_2, s_0, s_1, s_2,$ and γ are the ρ_∞ -Bathe parameters and \mathbf{U} and Δt are a vector of the solution and the time step size, respectively. Using the above relations, the numerical solution of Eq. (8) can be obtained as

$$\begin{bmatrix} \ddot{\mathbf{x}}(t + \Delta t) \\ \dot{\mathbf{x}}(t + \Delta t) \\ \mathbf{x}(t + \Delta t) \end{bmatrix} = \mathbf{A} \begin{bmatrix} \ddot{\mathbf{x}}(t) \\ \dot{\mathbf{x}}(t) \\ \mathbf{x}(t) \end{bmatrix} = \frac{1}{\kappa_1 \kappa_2} \begin{bmatrix} a_{11} & a_{12} & a_{13} \\ a_{21} & a_{22} & a_{23} \\ a_{31} & a_{32} & a_{33} \end{bmatrix} \begin{bmatrix} \ddot{\mathbf{x}}(t) \\ \dot{\mathbf{x}}(t) \\ \mathbf{x}(t) \end{bmatrix} \quad (13)$$

where

$$\begin{aligned} a_{11} &= -k_0^2 c_0^2 \Delta t^2 (\gamma^2 q_2 (s_0 - s_1) k_0^2 c_0^2 \Delta t^2 + 2(q_1 \gamma + 2q_2 s_0)); \\ a_{12} &= -k_0^2 c_0^2 \Delta t ((q_0 - q_1 + q_2) \gamma - 4s_1 q_2) \gamma k_0^2 c_0^2 \Delta t^2 + 4(q_0 + q_1 + q_2); \\ a_{13} &= -k_0^2 c_0^2 (4 + (\gamma^2 - 2q_1 \gamma - 4s_1 q_2) k_0^2 c_0^2 \Delta t^2); \\ a_{21} &= -\Delta t (\gamma((-s_0 + s_1) \gamma + 2s_2 q_1) k_0^2 c_0^2 \Delta t^2 - 4s_0); \\ a_{22} &= 4 - \gamma^2 s_2 (q_0 - q_1) k_0^4 c_0^4 \Delta t^4 + (\gamma^2 - 4s_1 \gamma - 4s_2 (q_0 + q_1)) k_0^2 c_0^2 \Delta t^2; \\ a_{23} &= k_0^2 c_0^2 \Delta t (s_2 \gamma (2q_1 - \gamma) k_0^2 c_0^2 \Delta t^2 - 4(s_1 + s_2)); \\ a_{31} &= -a_{11} / k_0^2 c_0^2; a_{32} = -a_{12} / k_0^2 c_0^2; a_{33} = -a_{13} / k_0^2 c_0^2; \\ \kappa_1 &= \gamma^2 k_0^2 c_0^2 \Delta t^2 + 4; \text{ and } \kappa_2 = q_2 s_2 k_0^2 c_0^2 \Delta t^2 + 1; \end{aligned} \quad (14)$$

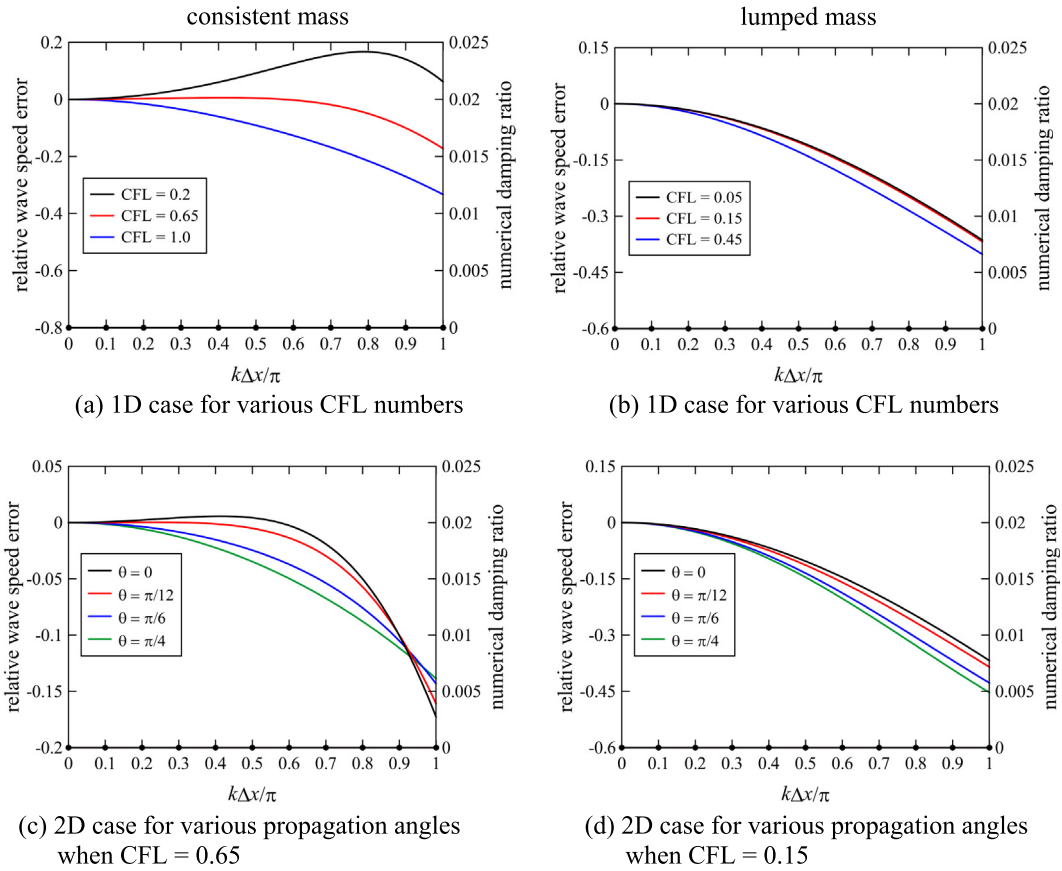


Fig. 11. Relative wave speed errors (left axis) and numerical damping (right axis) of the trapezoidal rule with the consistent and lumped mass matrices; results for solid line are relative wave speed errors; and results for marked lines are the numerical damping ratio.

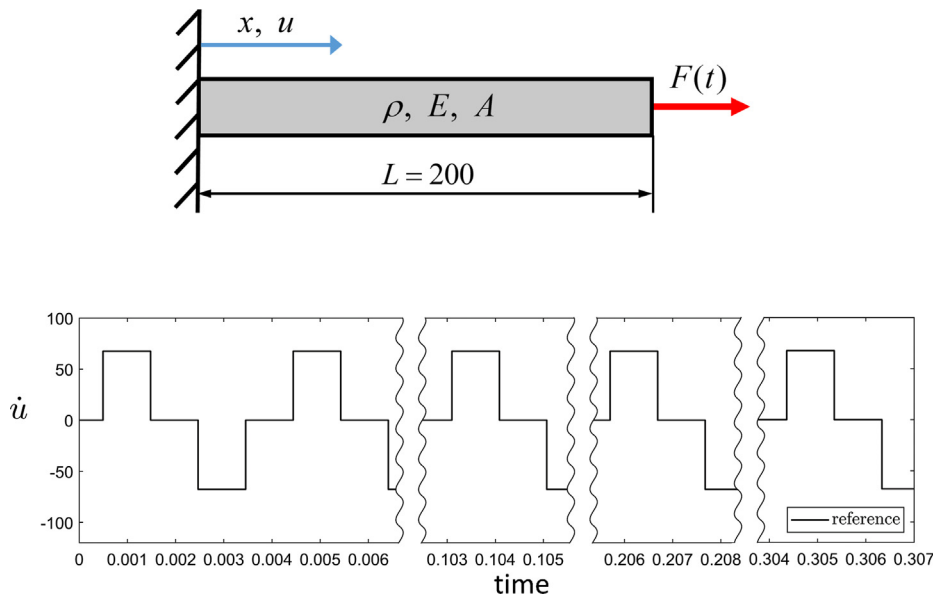


Fig. 12. A clamped bar excited by a step load, and the exact velocity at the center, $x = 100$. Young's modulus $E = 3 \times 10^7$, mass density $\rho = 0.00073$, cross-sectional area $A = 1$, length $L = 200$ [36]. The receiver is located at the center.

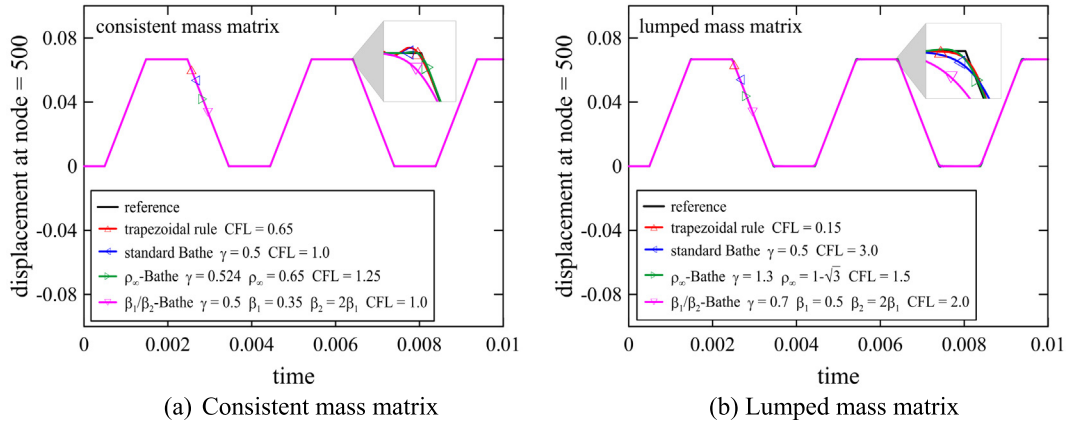


Fig. 13. Time history of displacements at the center of the bar using various Bathe time integration schemes and trapezoidal rule.

To have second-order accuracy, unconditional stability with the complex conjugate eigenvalues for all time step sizes, we use

$$q_1 = s_1 = \frac{\rho_\infty + 1}{2\gamma(\rho_\infty - 1) + 4};$$

$$q_0 = s_0 = (\gamma - 1)q_1 + \frac{1}{2}; \quad \text{and} \quad q_2 = s_2 = -\gamma q_1 + \frac{1}{2} \quad (15)$$

Thus, the scheme has two parameters, $\gamma > 0$ and $\rho_\infty \in (-1, 1]$ [36]. The scheme provides a local maximum for the amplitude decay and the global minimum of period elongation with an identical effective stiffness matrix for each sub-step by using $\rho_\infty \in [0, 1]$ and the following value of γ

$$\gamma_0 = \frac{2 - \sqrt{2 + 2\rho_\infty}}{1 - \rho_\infty}; \quad \gamma_0 = 0.5 \quad \text{if} \quad \rho_\infty = 1 \quad (16)$$

Note that if $\rho_\infty = 0$ the standard Bathe scheme is obtained using only one effective stiffness matrix with Eq.(16), that is, $\gamma_0 = 2 - \sqrt{2}$ [25,26]. Table 1 summarizes some important uses of the parameters in the ρ_∞ -Bathe scheme for various problem solutions.

The method reduces to the β_1/β_2 -Bathe scheme with the following relations

$$q_0 = s_0 = \gamma(1 - \beta_1); \quad q_1 = s_1 = \gamma(\beta_1 + \beta_2 - 1) + 1 - \beta_2; \quad \text{and}$$

$$q_2 = s_2 = (1 - \gamma)\beta_2 \quad (17)$$

Also, the ρ_∞ -Bathe method includes the Newmark method as a special case in that it reduces to the two-step Newmark method with $\alpha = 0.25(\delta + 0.5)^2$ using the following relations

$$q_0 = s_0 = \frac{-4\delta^2 + 12\delta - 1}{16\delta + 8}, \quad q_1 = s_1 = \frac{1}{2\delta + 1},$$

$$q_2 = s_2 = \frac{2\delta + 1}{8}, \quad \gamma = \frac{2\delta + 1}{4} \quad (18)$$

We refer to Ref. [36] for discussions on the relationship between the ρ_∞ -Bathe and Newmark schemes. But we recall that the Newmark method is only first-order accurate unless used as the trapezoidal rule whereas the ρ_∞ -Bathe scheme is second-order accurate for all ρ_∞ and γ (as used in the illustrative solutions below).

With the relations in Eq. (17), the β_1/β_2 -Bathe method has three parameters: β_1 , β_2 and γ . The values $\beta_2 = 1 - \beta_1$ and $\beta_2 = 2\beta_1$, both with $\gamma = 0.5$, have been used in Ref. [35]. In the present study, we consider the dispersion of the β_1/β_2 -Bathe method for various

$\gamma > 0$ using $\beta_2 = 2\beta_1$ since the β_1/β_2 -Bathe method with $\beta_2 = 1 - \beta_1$ provides the same characteristics as the ρ_∞ -Bathe method with the relations in Eqs. (15) and (16). Hereafter, we imply that in the β_1/β_2 -Bathe method we always use $\beta_2 = 2\beta_1$.

The characteristic polynomial of the integration approximation matrix **A** in Eq. (13) is

$$p(\eta) = \eta^3 - 2A_1\eta^2 + A_2\eta - A_3 \quad (19)$$

where

$$A_1 = (a_{11} + a_{22} + a_{33})/(\kappa_1\kappa_2);$$

$$A_2 = (a_{11}a_{22} + a_{22}a_{33} + a_{33}a_{11} - a_{12}a_{21} - a_{23}a_{32} - a_{31}a_{13})/(\kappa_1\kappa_2)^2; \quad \text{and}$$

$$A_3 = 0 \quad (20)$$

The eigenvalues of **A** are $|\eta_1|, |\eta_2| \leq 1$ and $\eta_3 = 0$ for all time step sizes Δt . With Eqs. (8) and ((13), (14)), we obtain the following expression

$$x(t + 2\Delta t) - 2A_1x(t + \Delta t) + A_2x(t) = 0 \quad (21)$$

We now assume that the numerical solution of Eq. (8) is given by

$$x(t) = d_1e^{(-\xi+i)kct} + d_2e^{(-\xi-i)kct} \quad (22)$$

where d_1, d_2 , and c are undetermined coefficients and the numerical wave speed, and the numerical damping ratio [29] is

$$\xi = -\frac{1}{2k_0c_0\Delta t} \ln(A_2) \quad (23)$$

Substituting Eqs. (22) and (23) into Eq. (21) with the relation between k and k_0 obtained through Eq. (7), we finally obtain the total dispersion error, the relation between c/c_0 , k and the CFL number ($c_0\Delta t/h$), where h is the ‘‘characteristic element length’’.

A key point is that when using a dissipative time integration method, we aim to eliminate unwanted (highly inaccurate) wave modes in the numerical solutions. We estimate the discarded wave modes using the relationship between the CFL number, $k\Delta x$, and $\omega\Delta t$

$$k\Delta x = \frac{c_0}{c} \frac{\Omega}{\text{CFL}} \quad (24)$$

where $\Omega = \omega\Delta t$ and ω is the numerical natural frequency obtained from [29]

$$\Omega = \begin{cases} \arctan\left(\sqrt{A_2 - A_1^2}/A_1\right) & \text{for } \Delta t \leq \Delta t^* \\ \arctan\left(-\sqrt{A_2 - A_1^2}/A_1\right) & \text{for } \Delta t > \Delta t^* \end{cases} \quad (25)$$

where $A_2 - A_1^2|_{\Delta t = \Delta t^*} = 0$.

When using the standard Bathe method, the wave modes with $\Delta t/T > 0.3$ are discarded in the numerical solution due to numerical damping [45]. We use this fact to identify the practically discarded wave modes in the dispersion analysis below.

In the next section, we analyze the dispersion properties of the ρ_∞ -Bathe scheme with $\rho_\infty \in [0, 1]$ using $0 < \gamma < 1$ and $1 < \gamma < 2/(1 - \rho_\infty)$ since $\gamma = 0, 1, 2/(1 - \rho_\infty)$ give zero denominators of constants in the ρ_∞ -Bathe scheme [24]. The scheme may provide less period elongation and larger dissipation for low-frequency modes with $\rho_\infty \in (-1, 1 - \sqrt{3})$ and $\gamma > 1$ than the scheme with $\rho_\infty \in [0, 1]$ and $0 < \gamma < 1$ [36]. Therefore, we also analyze the method with $\rho_\infty \in (-1, 1 - \sqrt{3})$ using $1 < \gamma \leq 1.5774$ and note that for $\gamma \in [1.5744, \infty)$ the method has its counterpart with identical spectral properties in $\gamma \in (1, 1.5744]$ [36].

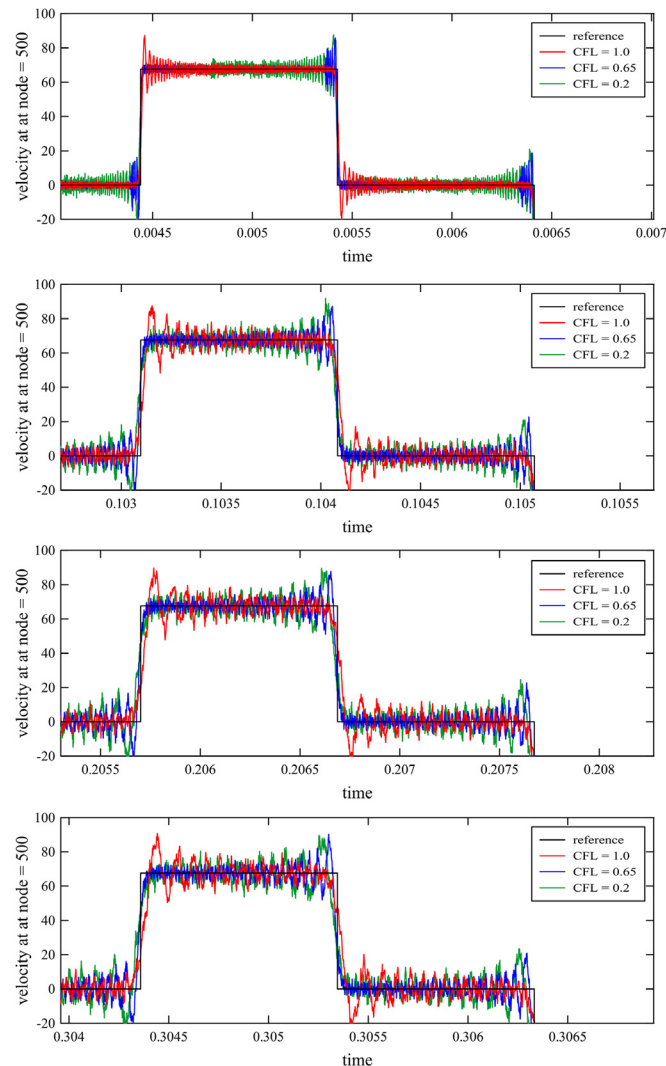


Fig. 14. Time history of velocities at the center of the bar using the trapezoidal rule with the consistent mass matrix.

In ref. [34], the stability and accuracy characteristics of the β_1/β_2 -Bathe scheme were analyzed using $\gamma = 0.5$. Below, we examine the dispersion properties of the β_1/β_2 -Bathe scheme using various positive values of $\beta_1 \geq 0.25$ (with $\beta_2 = 2\beta_1$) and $\gamma \neq 1$, for which the method is unconditionally stable (see Fig. 1 and Appendix A).

In Figs. 2–11, we present the total dispersion errors (represented by the errors in the wave speeds) and the numerical damping of various time integrations with the standard displacement-based spatial discretization. We consider that the optimal values of parameters of an integration scheme are those values, which for the largest CFL number give almost zero dispersion error for the resolved, participating, modes and “good” numerical damping for the higher modes that spatially cannot be resolved. The resolved modes shall be all modes of wavelengths larger than (about) 4 times the “effective element size”, and the spatially non-resolved modes shall be rapidly damped out of the solution [3]. Hence while the error in the wave speed shall be very small for all waves with (about) $k\Delta x/\pi \leq 0.5$, the numerical damping ratio shall increase continuously and rapidly for all waves with (about) $k\Delta x/\pi > 0.5$.

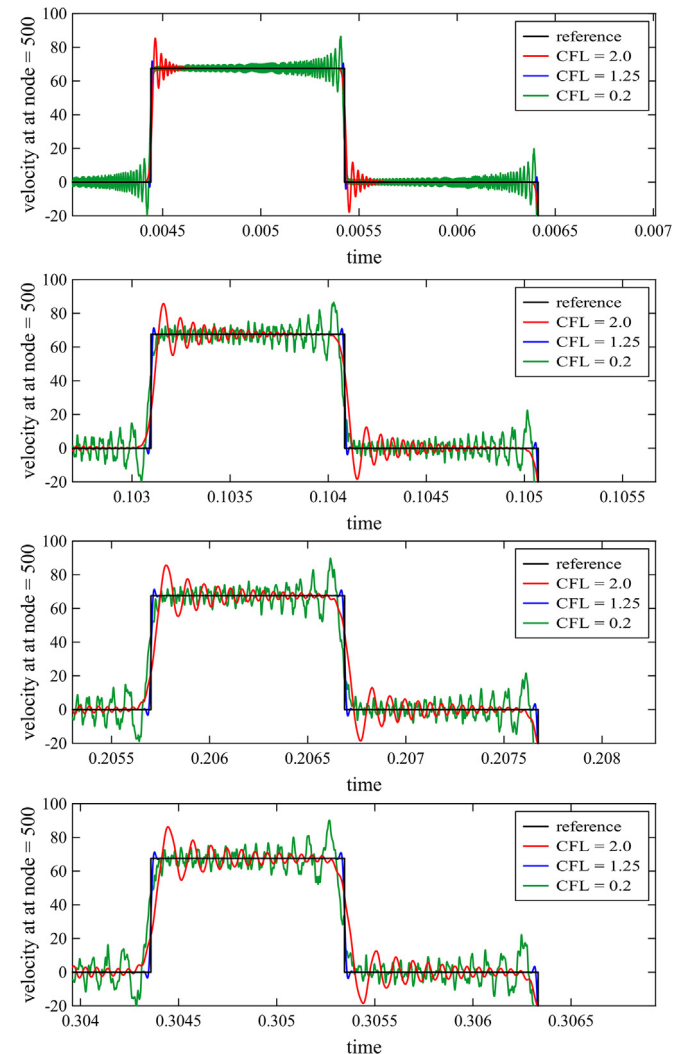


Fig. 15. Time history of velocities at the center of the bar using the ρ_∞ -Bathe time integration scheme with the consistent mass matrix ($\rho_\infty = 0.65$ and $\gamma = \gamma_0$).

2.1. Dispersion analysis in the 1D case

In the one-dimensional case, the rows of the matrices of consistent mass matrix $\mathbf{D}_{\text{mass,c}}$, lumped mass matrix $\mathbf{D}_{\text{mass,\ell}}$, and stiffness matrix $\mathbf{D}_{\text{stiff}}$ are

$$\text{Row}(\mathbf{D}_{\text{mass,c}}) = \frac{\Delta x}{6} [0 \ \dots \ 0 \ e^{-ik\Delta x} \ 4 \ e^{ik\Delta x} \ 0 \ \dots \ 0] \quad (26)$$

$$\text{Row}(\mathbf{D}_{\text{mass,\ell}}) = \Delta x [0 \ \dots \ 0 \ 0 \ 1 \ 0 \ 0 \ \dots \ 0] \quad (27)$$

$$\text{Row}(\mathbf{D}_{\text{stiff}}) = \frac{1}{\Delta x} [0 \ \dots \ 0 \ -e^{-ik\Delta x} \ 2 \ -e^{ik\Delta x} \ 0 \ \dots \ 0] \quad (28)$$

In general, consistent and lumped mass matrices are used, respectively, with an implicit and explicit method [18]. However, it is also of interest to investigate finite element solutions calculated using explicit methods with a consistent mass matrix and solutions calculated using implicit methods with a lumped mass matrix [32,34,35,41,44].

2.1.1. The case of the consistent mass matrix

Using Eqs. (26) and (28) and the time integration scheme equations, the relative wave speed errors $(c - c_0)/c_0$ of the time integra-

tion methods are obtained corresponding to the normalized numerical wave number $k\Delta x/\pi (= \Delta x/(\lambda/2))$, where λ is the wave length.

Figs. 2–5 show the relative wave speed errors and numerical damping ratio of the ρ_∞ -Bathe method with the consistent mass matrix for some values of γ , ρ_∞ , and CFL. The overall conclusion of the study is that considering $\rho_\infty \in [0, 1]$ with $0 < \gamma < 1$ and $1 < \gamma < 2/(1 - \rho_\infty)$, we have good solution characteristics and solution cost at γ_0 with CFL=1. The same holds when $\rho_\infty \in (-1, 1 - \sqrt{3}]$ with $1 < \gamma \leq 1.5774$ for $\gamma = \gamma_p$ and CFL=0.75 where $\gamma_p = (\rho_\infty + 2 - \sqrt{\rho_\infty^2 - 2\rho_\infty - 2})/(3(\rho_\infty + 1))$ [36]. We also note that γ_0 and γ_p provide the least period elongations for low-frequency modes with $\rho_\infty \in [0, 1]$ and $\rho_\infty \in (-1, 1 - \sqrt{3}]$, respectively. And for the same $|\rho_\infty|$, using $\rho_\infty \in [0, 1]$ with γ_0 provides a larger optimal CFL number with more participating modes than using $\rho_\infty \in (-1, 1 - \sqrt{3}]$ with γ_p while the maximum dispersion errors are similar for both cases.

We conclude that therefore, when using the consistent mass matrix, it is best to use $\rho_\infty \in [0, 1]$ with γ_0 .

The range of the discarded wave modes decreases with an increase in $|\rho_\infty|$. However, for larger values of $|\rho_\infty|$, larger dispersion errors occur. Therefore, for general use in the solution of wave propagation problem, we suggest $(\rho_\infty, \gamma, \text{CFL}) = (0.65, \gamma_0, 1.25)$, see

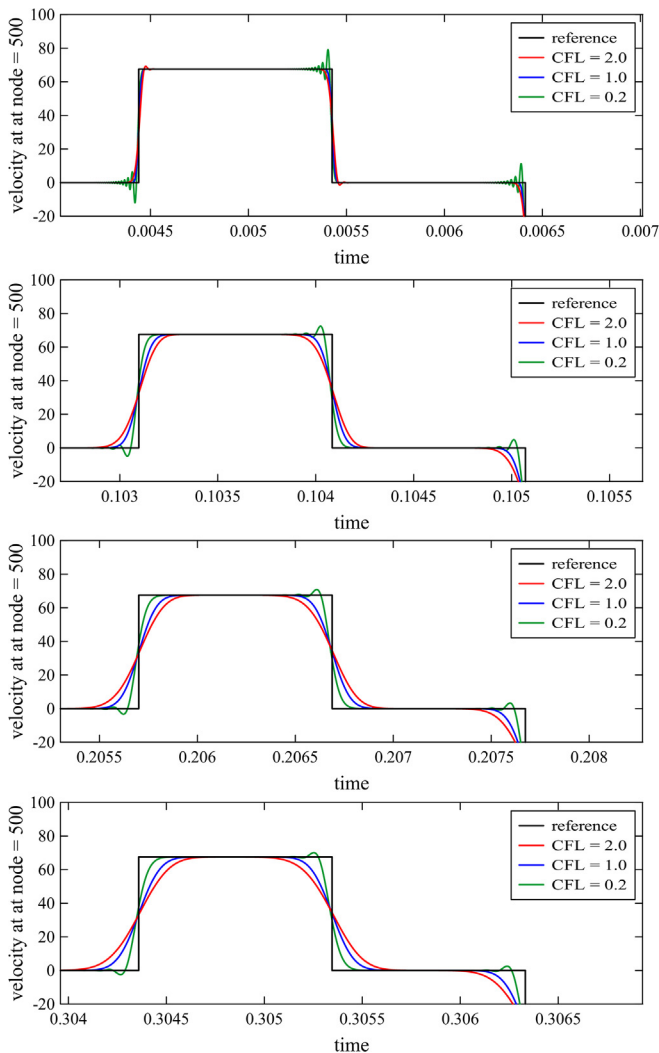


Fig. 16. Time history of velocities at the center of the bar using the β_1/β_2 -Bathe time integration scheme with the consistent mass matrix ($\beta_1 = 0.35$, $\beta_2 = 0.7$, and $\gamma = 0.5$).

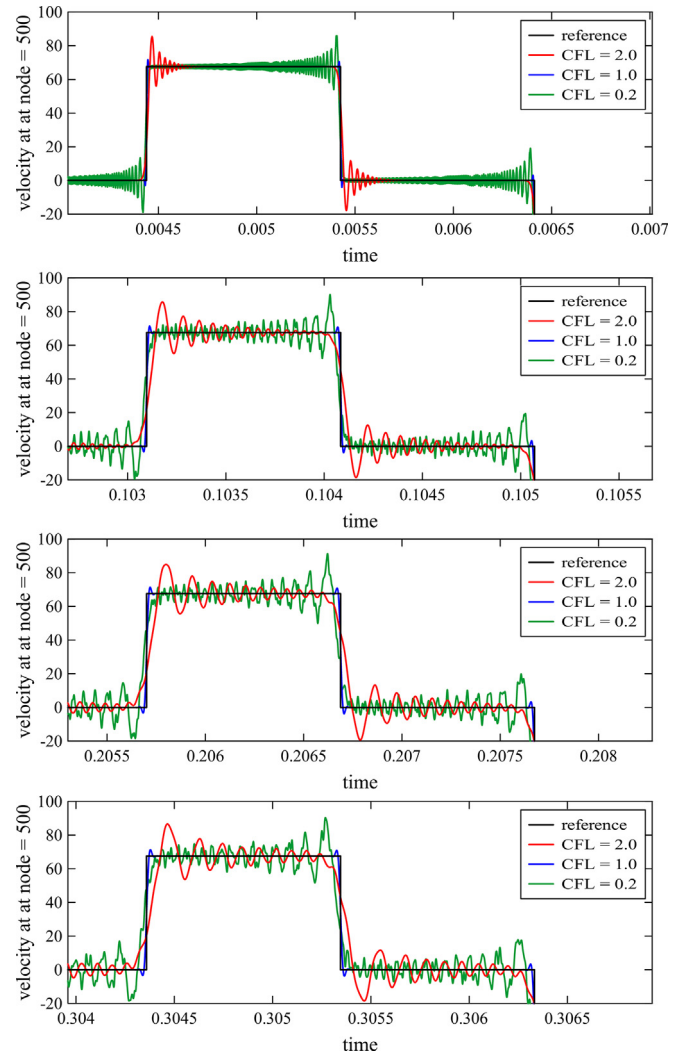


Fig. 17. Time history of velocities at the center of the bar using the standard Bathe time integration scheme with the consistent mass matrix.

Fig. 3. This setting provides similar dispersion properties as the standard Bathe method at its best use (with $\gamma = \gamma_0$ and CFL = 1) while requiring less (but only about 20% less) computational effort due to the larger CFL number.

Figs. 6 and 7 show the dispersion errors and numerical damping ratio of the β_1/β_2 -Bathe scheme with the consistent mass matrix for various values of γ , β_1 , and CFL. In the β_1/β_2 -Bathe scheme with $\beta_2 = 2\beta_1$, the parameter set $(\beta_1, \gamma) \approx (1/3, \gamma_{s1})$ is useful. However, the method is only first-order accurate and the solution errors in wave propagations become large at longer solution times, for an example solution see [Section 3.1](#).

2.1.2. Lumped mass matrix

To analyze the dispersion properties when using the lumped mass matrix, Eq. (27) is used instead of Eq. (26), and the dispersion analysis is performed as in the case of using the consistent mass matrix.

Fig. 8 shows the relative wave speed errors and numerical damping ratio of the ρ_∞ -Bathe method with the lumped mass matrix for some useful parameter sets in the range of $\rho_\infty \in [0, 1]$ with $\gamma < 1$ and $\rho_\infty \in (-1, 1 - \sqrt{3}]$ with $\gamma > 1$, for various CFL. With the optimal parameter sets, the ρ_∞ -Bathe scheme using the lumped mass matrix has larger wave speed errors than using the

consistent mass matrix. The dispersion curves show that when using the lumped mass matrix, the parameter set $(\rho_\infty, \gamma, CFL) = (1 - \sqrt{3}, 1.3, 1.5)$ might be used.

In the case of the β_1/β_2 -Bathe scheme with $\beta_2 = 2\beta_1$ and the lumped mass, the dispersion errors and numerical damping ratio are shown in **Fig. 14** for various values of γ , β_1 , and CFL number. These figures suggest setting $(\beta_1, \beta_2, \gamma, CFL) = (0.5, 1.0, 0.7, 2)$ but since the method is only first order accurate, it is overall more effective to use the ρ_∞ -Bathe scheme with the parameters given above.

2.2. Dispersion analysis in the 2D case

In the 2D case, the rows of the consistent mass matrix $\mathbf{D}_{mass,c}$, lumped mass matrix $\mathbf{D}_{mass,\ell}$, and stiffness matrix \mathbf{D}_{stiff} are:

$$\text{Row}(\mathbf{D}_{mass,c}) = \frac{h^2}{36} [0 \ \dots \ 0 \ \mathbf{D}_{mass,c,sub1} \ 16 \ \mathbf{D}_{mass,c,sub2} \ 0 \ \dots \ 0] \tag{29}$$

$$\text{Row}(\mathbf{D}_{mass,\ell}) = h^2 [0 \ \dots \ 0 \ 0 \ 0 \ 0 \ 0 \ 1 \ 0 \ 0 \ 0 \ 0 \ \dots \ 0] \tag{30}$$

$$\text{Row}(\mathbf{D}_{stiff}) = \frac{1}{3} [0 \ \dots \ 0 \ \mathbf{D}_{stiff,sub1} \ 8 \ \mathbf{D}_{stiff,sub2} \ 0 \ \dots \ 0] \tag{31}$$

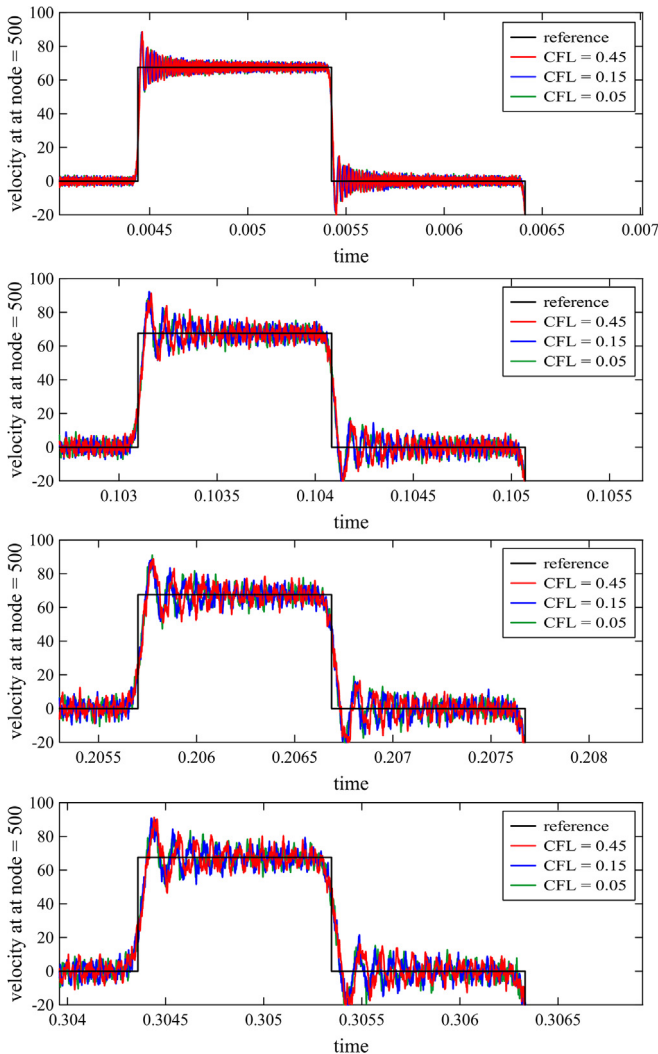


Fig. 18. Time history of velocities at the center of the bar using the trapezoidal rule with the lumped mass matrix.

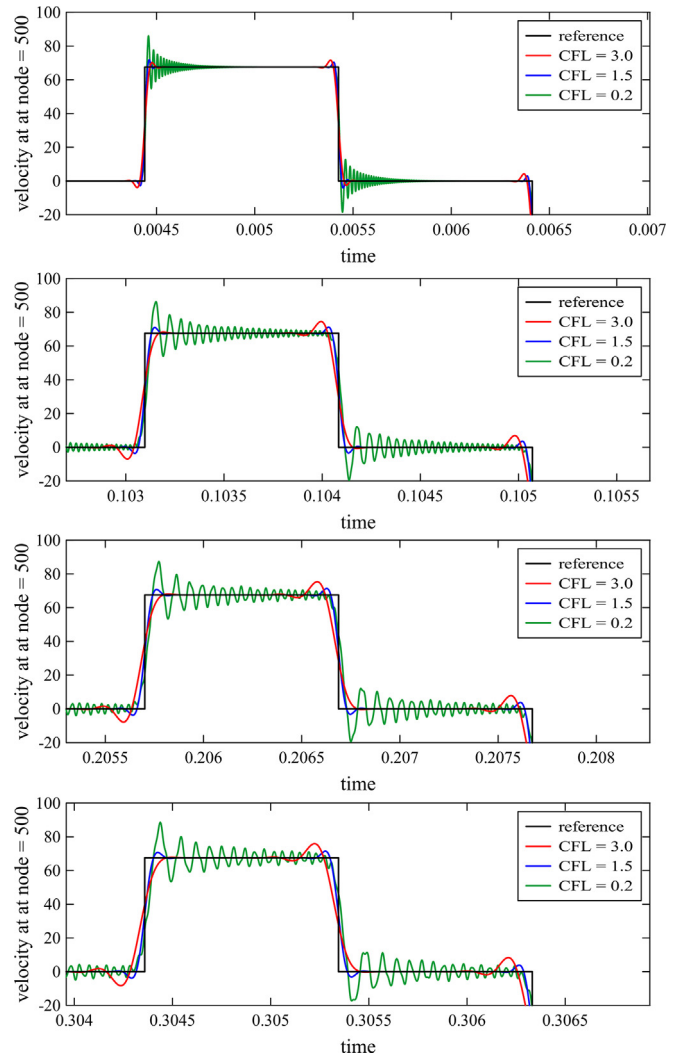


Fig. 19. Time history of velocities at the center of the bar using the ρ_∞ -Bathe time integration scheme with the lumped mass matrix ($\rho_\infty = 1 - \sqrt{3}$ and $\gamma = 1.3$).

where

$$\mathbf{D}_{\text{mass,c.sub1}} = \begin{bmatrix} e^{-ik\Delta x(\cos\theta+\sin\theta)} & 4e^{-ik\Delta x\sin\theta} & e^{ik\Delta x(\cos\theta-\sin\theta)} & 4e^{-ik\Delta x\cos\theta} \end{bmatrix} \tag{32}$$

$$\mathbf{D}_{\text{mass,c.sub2}} = \begin{bmatrix} 4e^{ik\Delta x\cos\theta} & e^{ik\Delta x(-\cos\theta+\sin\theta)} & 4e^{ik\Delta x\sin\theta} & e^{ik\Delta x(\cos\theta+\sin\theta)} \end{bmatrix} \tag{33}$$

$$\mathbf{D}_{\text{stiff.sub1}} = \begin{bmatrix} -e^{-ik\Delta x(\cos\theta+\sin\theta)} & -e^{-ik\Delta x\sin\theta} & -e^{ik\Delta x(\cos\theta-\sin\theta)} & -e^{-ik\Delta x\cos\theta} \end{bmatrix} \tag{34}$$

$$\mathbf{D}_{\text{stiff.sub2}} = \begin{bmatrix} -e^{ik\Delta x\cos\theta} & -e^{ik\Delta x(-\cos\theta+\sin\theta)} & -e^{ik\Delta x\sin\theta} & -e^{ik\Delta x(\cos\theta+\sin\theta)} \end{bmatrix} \tag{35}$$

where θ is the angle between the direction of wave propagation and the x axis.

We use Eqs. (29)–(31) instead of Eqs. (26)–(28) to analyze the dispersion properties, like we considered the 1D case, and for both the consistent and lumped mass matrices.

Fig. 10 shows the relative wave speed errors and numerical damping ratio of the Bathe time integration schemes for various values of the propagation angle. The 1D and 2D dispersion curves for the trapezoidal rule with its useful CFL numbers for the consis-

tent and lumped mass matrices are shown in Fig. 11 [45]. The figures show that the use of the ρ_∞ -Bathe scheme with $(\rho_\infty, \gamma, \text{CFL}) = (0.65, \gamma_0, 1.25)$ and the standard Bathe scheme, both used with the consistent mass matrix, are effective. We arrive at this conclusion also in Section 3.1.

3. Wave propagation solutions

In this section, we present several wave propagation solutions to illustrate the performance of the schemes with consistent and lumped mass matrices. We consider three cases: a 1D wave propagation problem, a 2D transient scalar wave propagation problem, and a 2D elastic wave propagation problem.

To demonstrate the effect of the parameters, we give solutions for some typical choices of parameters when using the consistent and lumped mass matrices.

3.1. A one-dimensional wave propagation problem

We consider the clamped-free bar shown in Fig. 12. An external step load $F(L, t) = 10,000$ is applied at the end of the bar, which has length $L = 200$, mass density $\rho = 7.3 \times 10^{-4}$, elastic modulus

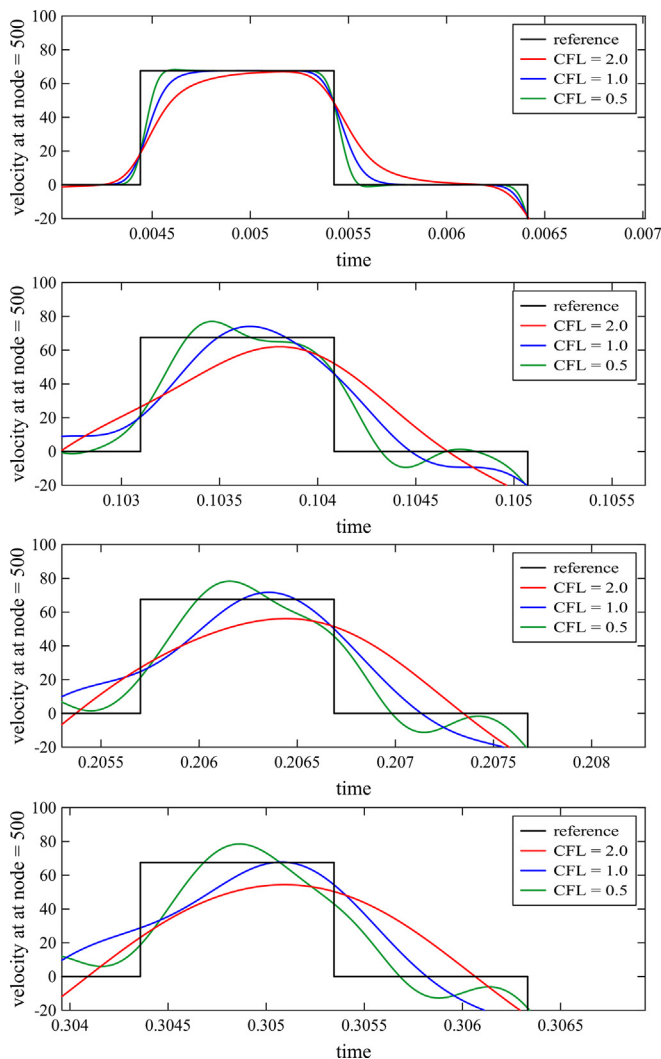


Fig. 20. Time history of velocities at the center of the bar using the ρ_∞ -Bathe time integration scheme with the lumped mass matrix ($\rho_\infty = 0$ and $\gamma = 1.99$).

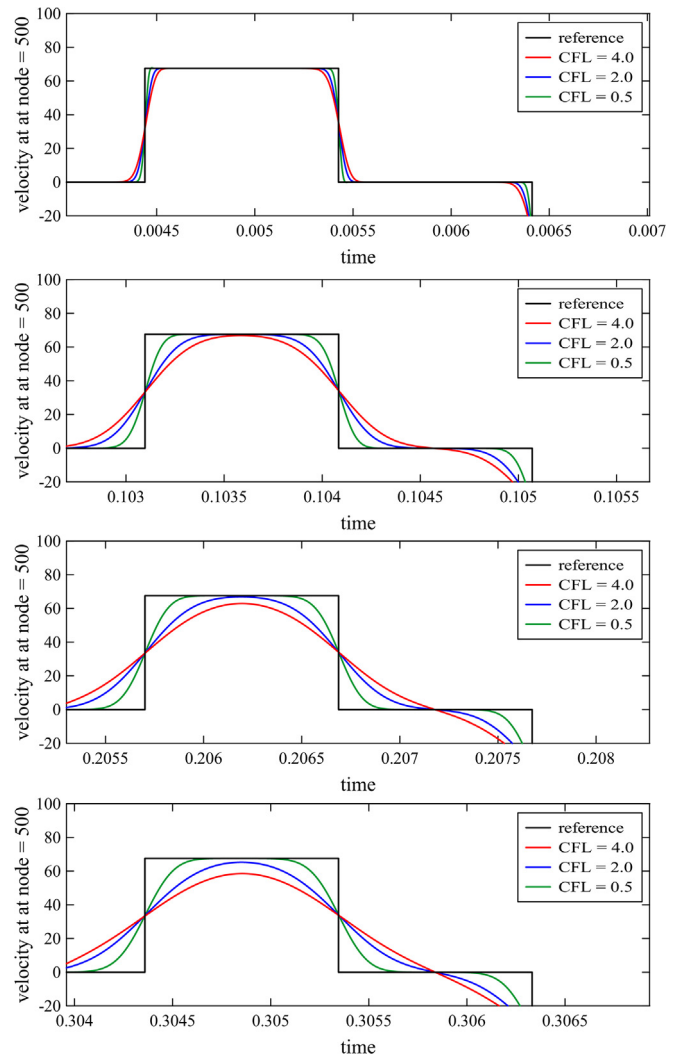


Fig. 21. Time history of velocities at the center of the bar using the β_1/β_2 -Bathe time integration scheme with the lumped mass matrix ($\beta_1 = 0.5$, $\beta_2 = 1.0$, and $\gamma = 0.7$).

$E = 3.0 \times 10^7$, and cross-sectional area $A = 1.0$. The number of equal-sized two-node elements N is set to 1000. This problem was also considered for solution in Refs. [34–36].

Fig. 13 shows the “early” time histories at node 500 (the center of the bar) of the displacement using the various solution schemes. All solutions are quite accurate, however, this accuracy is not seen when the predicted velocity is studied and at longer times.

Figs. 14–17 show the time history of velocities at node 500. With its best CFL numbers, the ρ_∞ - and standard Bathe schemes result in remarkably accurate solutions for all time windows while the β_1/β_2 -Bathe method, a first-order method, deteriorates in accuracy at larger times due to high numerical damping. The trapezoidal rule provides large numerical oscillations in all time windows, and does so for small and large CFL numbers.

Hence, although the Bathe schemes use two sub-steps per time step, and hence about twice the solution effort per time step than the trapezoidal rule, the accuracy reached with even a smaller computational effort is much better with the ρ_∞ -Bathe scheme.

Note that using the consistent mass matrix, the ρ_∞ -Bathe method with CFL = 1.25 and standard method with CFL 1.0 pro-

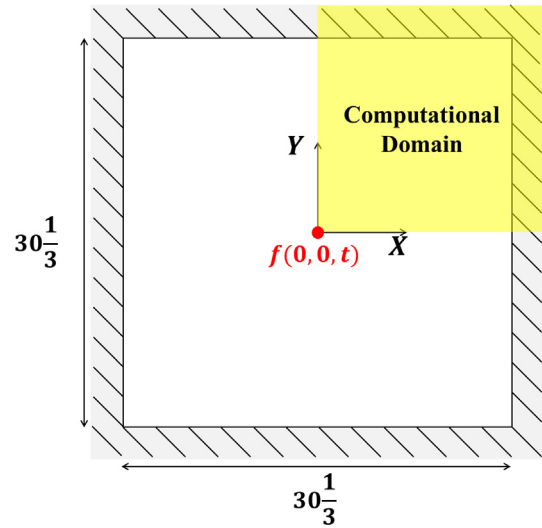


Fig. 23. 2D scalar wave propagation problem: a pre-stressed membrane; the origin of Cartesian coordinate system is located at the center of the membrane.

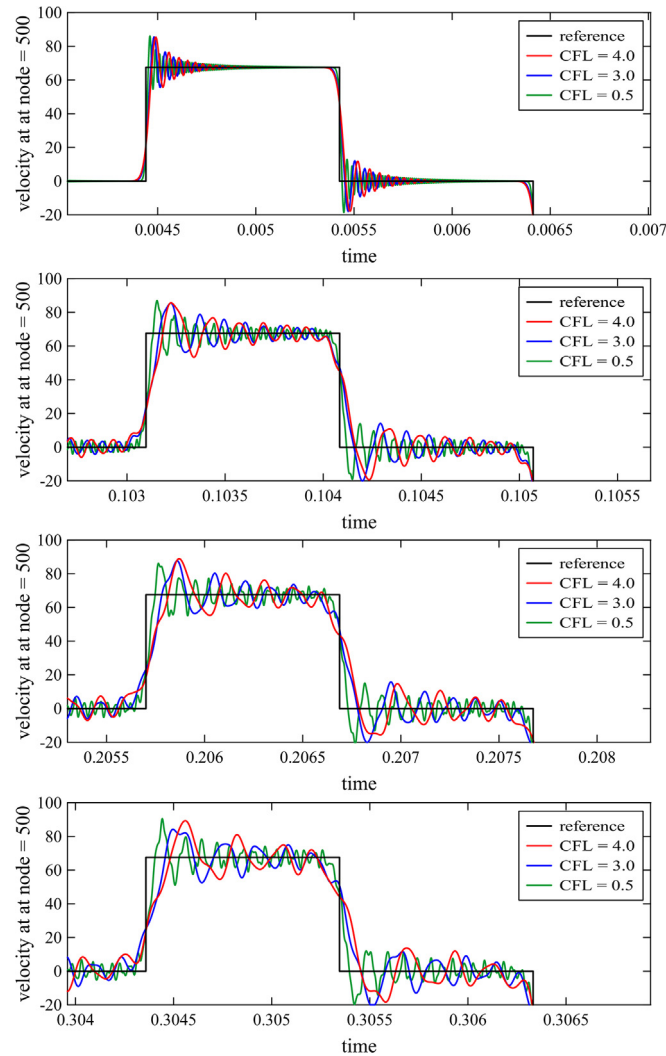


Fig. 22. Time history of velocities at the center of the bar using the standard Bathe time integration scheme with the lumped mass matrix.

vides very similar results. Therefore, to reduce the computational cost, the ρ_∞ -Bathe scheme using $\rho_\infty = 0.65$ and CFL = 1.25 with the consistent mass is most effective, but only slightly more effective than using the standard Bathe method with CFL = 1.0.

Figs. 18–22 show the results obtained using the lumped mass matrix. Here only the ρ_∞ -Bathe method with $(\rho_\infty, \gamma, CFL) = (1 - \sqrt{3}, 1.3, 1.5)$ provides satisfactory results for all time windows considered. We also see that overall, the use of the consistent mass matrix provides more accurate solutions than the use of the lumped mass matrix.

In the solutions given in the next sections, we only show the results obtained with the trapezoidal rule and the ρ_∞ - and standard Bathe schemes using the consistent mass and lumped mass matrices with their optimal CFL.

3.2. A two-dimensional scalar wave propagation problem

We consider the pre-stressed membrane shown in Fig. 23 [44,45,30]. The transverse displacement u , velocity \dot{u} , acceleration \ddot{u} are calculated solving the equation

$$\frac{1}{c_0^2} \frac{\partial^2 u}{\partial t^2} - \left(\frac{\partial^2 u}{\partial x^2} + \frac{\partial^2 u}{\partial y^2} \right) = f(0, 0, t) \tag{36}$$

where c_0 is the exact wave velocity. We use $c_0 = 1$ and impose zero initial displacement and velocity conditions. The concentrated load at the center of the membrane is given as

$$f(0, 0, t) = \begin{cases} 4(1 - (2t - 1)^2) & 0 < t < 1 \\ 0 & 1 \leq t \end{cases} \tag{37}$$

As there is symmetry about the x and y axes, the domain $[0, 15\frac{1}{6}]$ by $[0, 15\frac{1}{6}]$ is considered for the solution. We mesh the computational domain using a regular mesh of four-node elements with nodes equally spaced.

Figs. 24 and 25 show snapshots of the transverse displacements and velocities obtained using the consistent mass matrix for various meshes. In Fig. 26, the numerical results of displacements and velocities at two propagating angles using the

140 × 140 element mesh are compared with the analytical solution.

The ρ_∞ - and the standard Bathe methods provide similar results for all meshes, and the schemes provide reasonably accurate solutions when the 70 × 70 element mesh is used. While the solutions at the angle of $\theta = 0$ are quite accurate, noticeable distortions are

observed in the velocities at $\theta = \pi/4$ since the time step size is calculated using the optimal CFL number based on $\theta = 0$ i.e. for $h = \Delta x$. Note that for the propagating angle θ , “the effective element length” is reduced to $h\sqrt{1 - 2\cos^2\theta(1 - \cos^2\theta)}$ [45]. Therefore, if the time step size is based on h , the effective CFL number along the angle θ is larger and so is the wave speed error (see e.g. Fig. 3).

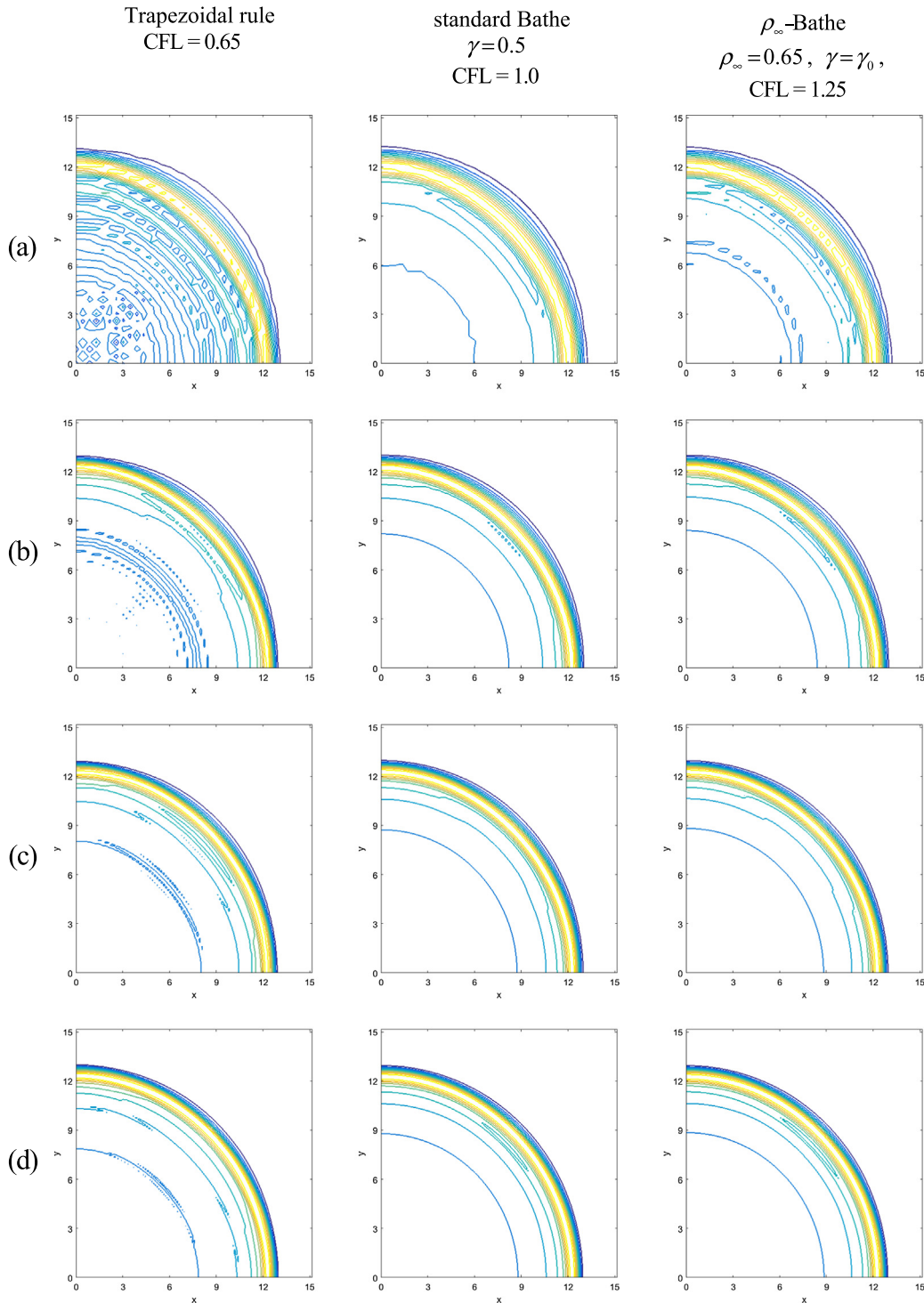


Fig. 24. Snapshot of displacements at time $t = 13$ for various Bathe schemes with consistent mass matrix: (a) 35 by 35, (b) 70 by 70, (c) 105 by 105, and (d) 140 by 140 finite element meshes.

The results using the trapezoidal rule for about the same solution effort are not as accurate.

When using the lumped mass matrix the results are considerably less accurate than when using the consistent mass matrix.

3.3. A two-dimensional elastic wave propagation problem

In this section, we provide the calculated response for the Lamb problem shown in Fig. 27 where multiple elastic waves are propagating in an elastic medium [30,44–46].

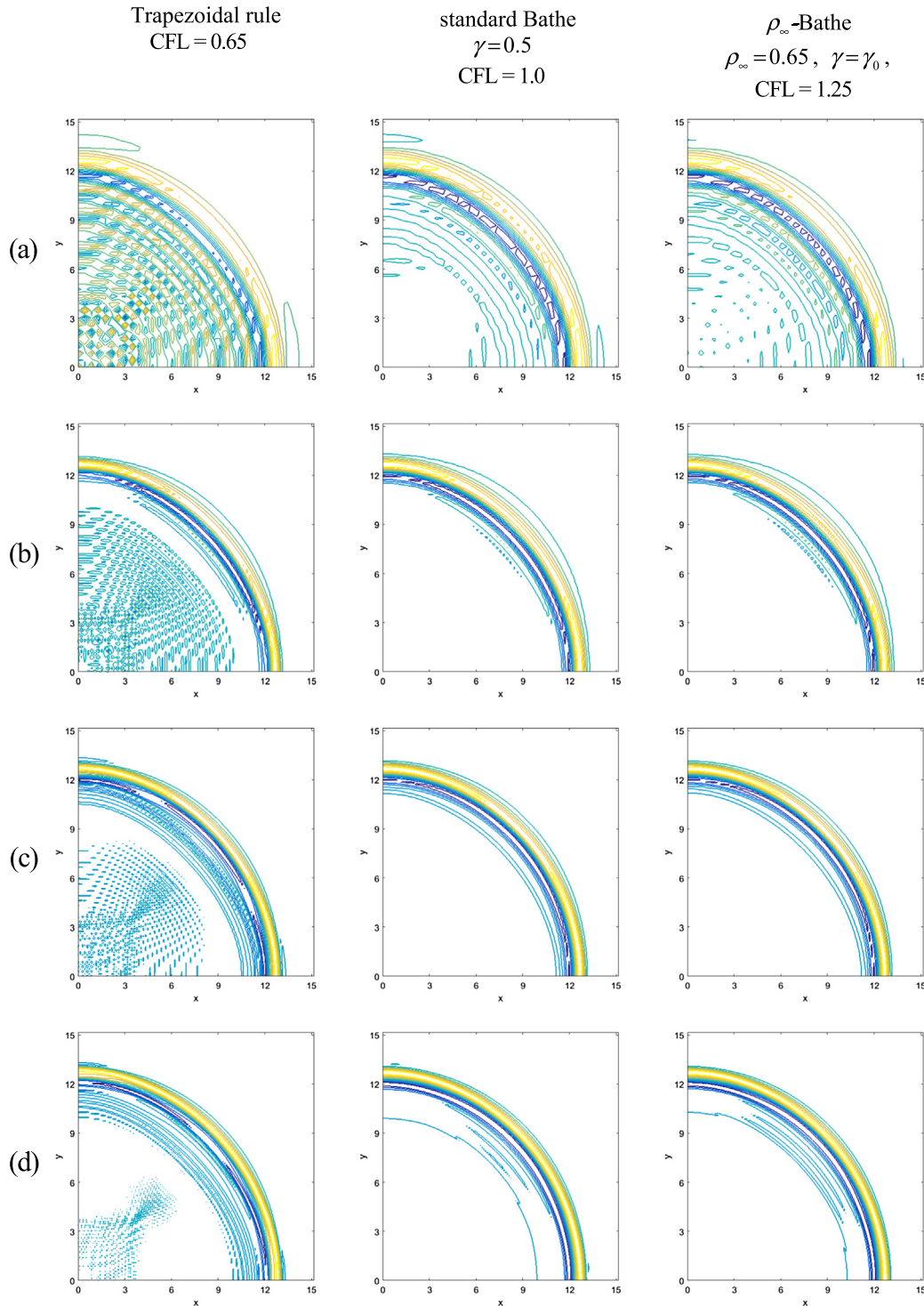


Fig. 25. Snapshot of velocities at time $t = 13$ for various Bathe schemes with consistent mass matrix: (a) 35 by 35, (b) 70 by 70, (c) 105 by 105, and (d) 140 by 140 finite element meshes.

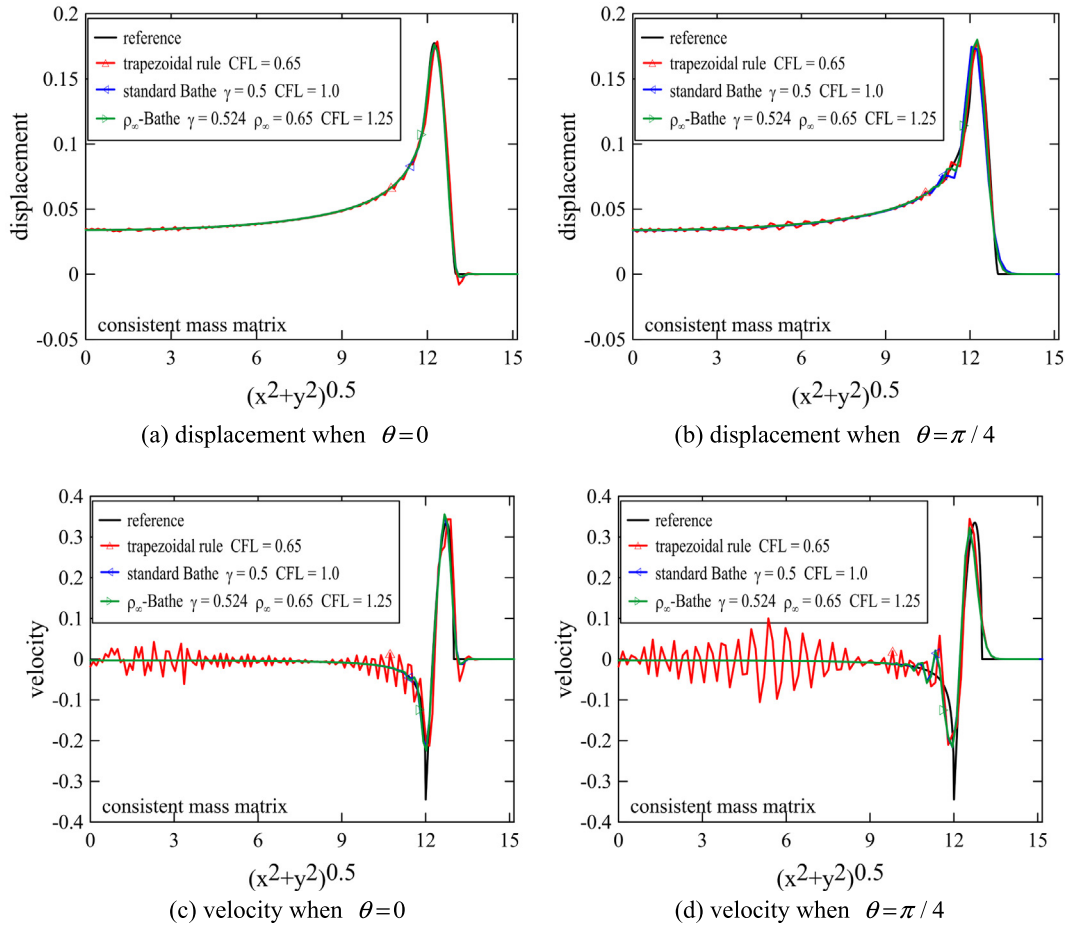


Fig. 26. Transverse displacements and velocities of the Bathe schemes and trapezoidal rule at time $t = 13$ and $t = 13.0271$, respectively, for the consistent mass matrix with 140 by 140 element mesh.

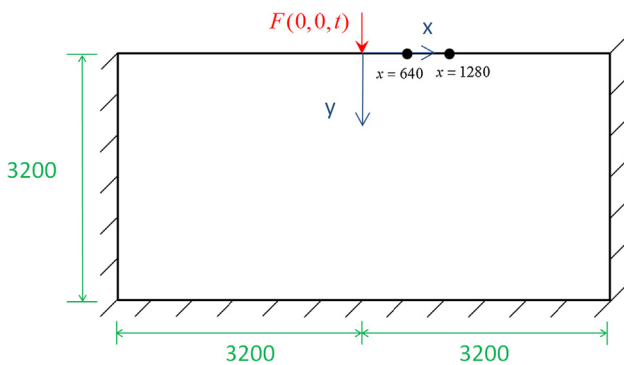


Fig. 27. 2D elastic wave propagation problem: A Lamb problem; two receivers are placed at $x = 640$ and $x = 1280$.

We use the mass density $\rho = 2200\text{kg/m}^3$, P-wave velocity $c_L = 3200\text{m/s}$, S-wave velocity $c_T = 1847.5\text{m/s}$, and $c_R = 1698.6\text{m/s}$, where c_R is the Rayleigh wave velocity. The time step sizes are calculated based on the P-wave velocity and the characteristic length, taken as the side length of the elements. We consider the numerical solutions of the displacements at two receivers located at $(x, y) = (640\text{m}, 0)$ and $(x, y) = (1280\text{m}, 0)$.

First, we apply the line force as a Ricker wavelet defined as follows:

$$f(0, 0, t) = -10^6 \times \left(1 - 2\pi^2 \hat{f}^2 (t - t_0)^2\right) e^{-\pi^2 \hat{f}^2 (t - t_0)^2}, \quad t > 0 \quad (38)$$

where the central frequency $\hat{f} = 12.5\text{Hz}$ and the time shift $t_0 = 0.1\text{ s}$. For this loading, we use the regular mesh of 1280×640 4-node finite elements (i.e. $\Delta x = \Delta y = 5\text{m}$).

Figs. 28 and 29 show the predicted displacements and the calculated von Mises stress at time $t \simeq 0.984\text{ s}$. The analytical solution and the numerical solutions using the Bathe schemes with the consistent mass matrix are in good agreement while the solutions obtained using the lumped mass matrix are not as accurate. Note that for the considered type of loading, the excited wave modes are quite limited, i.e. wave modes $k\Delta x/\pi \ll 1$ are excited; therefore the trapezoidal rule also provides similar solution accuracy (see Figs. 10 and 11).

We next consider the line force defined as follows:

$$f(0, 0, t) = 2 \times 10^3 \times [H(0.15 - t) - 3H(0.1 - t) + 3H(0.05 - t)], \quad t > 0 \quad (39)$$

where H is the Heaviside step function. This force consists of three step functions, which renders the problem more difficult to solve numerically. For the spatial discretization, we represent the computational domain using a mesh of 3200×1600 4-node finite elements (i.e. $\Delta x = \Delta y = 2\text{m}$).

Fig. 30 shows the horizontal and vertical displacements at the two receivers but obtained only with some solution parameters.

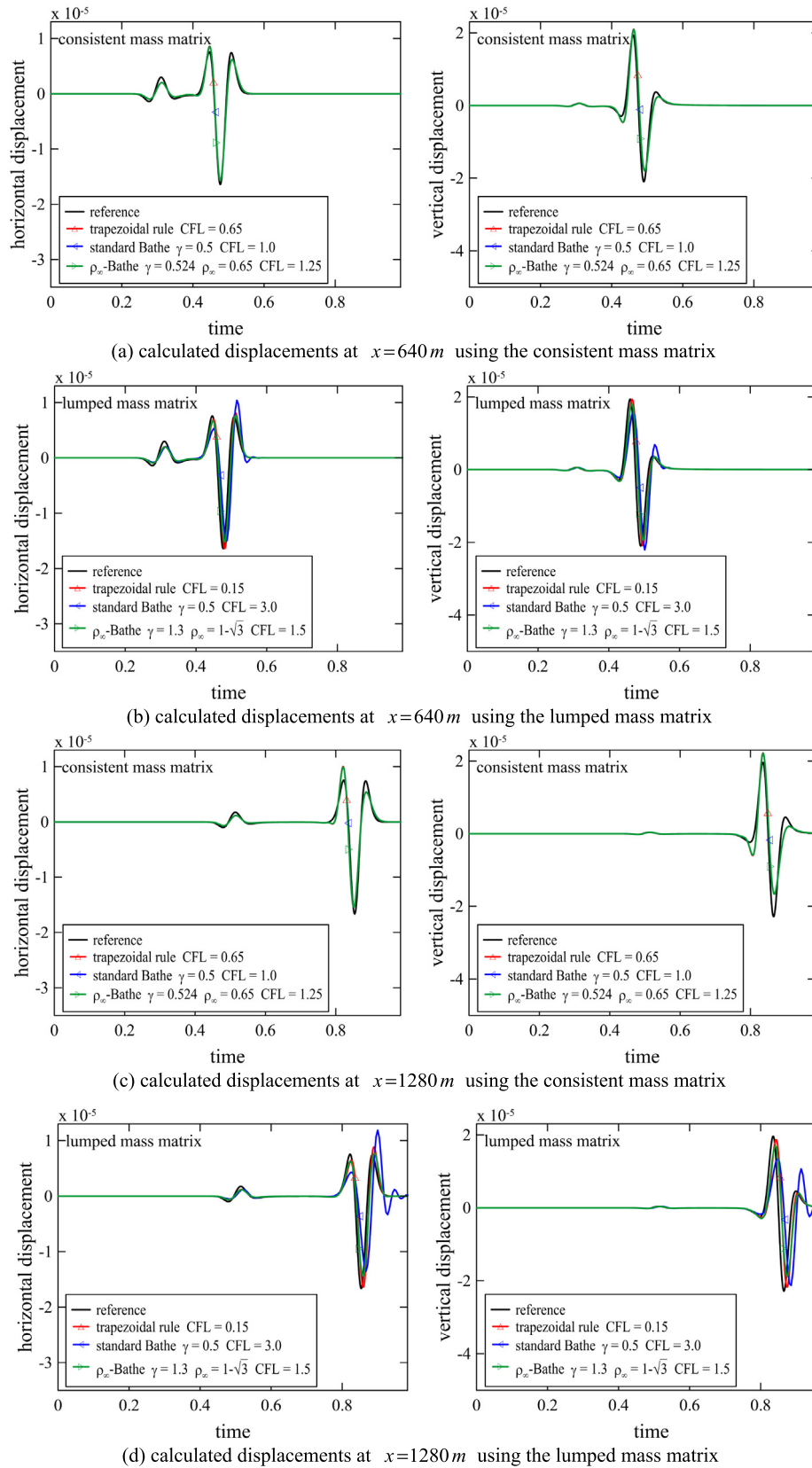


Fig. 28. Time history of horizontal displacements (left) and vertical displacements (right) with the regular mesh ($h = 5\text{ m}$) using various Bathe methods and trapezoidal rule when the Ricker wavelet line load is applied.

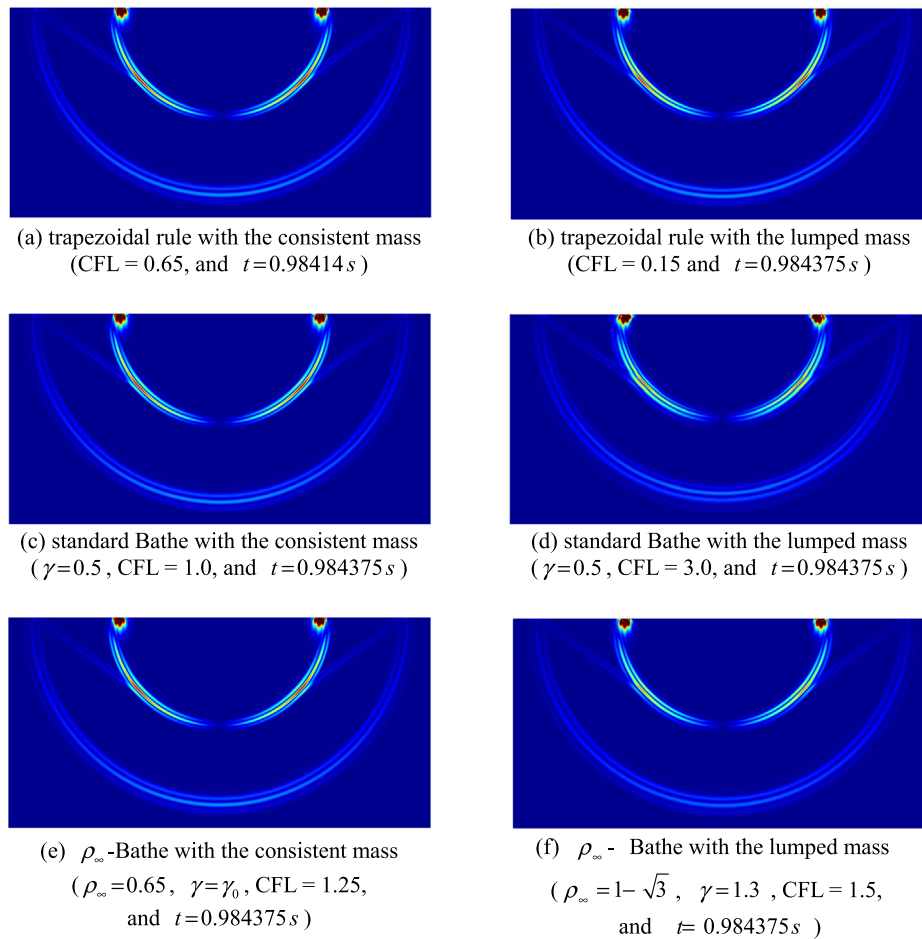


Fig. 29. Snapshot of von Mises stress using various Bathe methods and trapezoidal rule with the consistent mass matrix (left) and lumped mass matrix (right) when the Ricker wavelet line load is applied.

The calculated von Mises stress results over the complete mesh at $t \approx 0.937s$ are shown in Fig. 31. There are spurious oscillations in the solutions of the predicted horizontal and vertical displacements using all methods with the consistent mass matrix, and the trapezoidal rule and standard Bathe method with the lumped mass matrix. On the other hand, using the ρ_∞ -Bathe method with the lumped mass matrix provides reduced spurious oscillations. In this solution, some important wave modes are damped, hence the wave fronts are smoothed while the overall solution accuracy is enhanced compared to using the consistent mass matrix.

4. Concluding remarks

Our objective was to identify the optimal parameters and CFL numbers when using the Bathe implicit time integration methods for the solution of wave propagation problems with traditional finite element discretizations. These schemes include as special cases the trapezoidal rule and the Newmark method. To assess the accuracy of a scheme with a specific parameter set, we conducted dispersion and dissipation analyses.

We identified the optimal parameters and CFL numbers when a scheme is used with either the consistent or the lumped mass matrix. An important finding is that with the consistent mass matrix, the ρ_∞ -Bathe method with $\rho_\infty = 0.65$, $\gamma = \gamma_0$, and CFL = 1.25 and the standard Bathe method with $\gamma = 0.5$ and

CFL = 1.0 provide similar dispersion errors and numerical results in wave propagation analyses.

For the consistent mass matrix case, when using the Bathe schemes with the optimal parameters and CFL numbers, in essence, the wave modes with (about) $\Delta x/(\lambda/2) < 0.50$ participate in the numerical solutions whereas for the lumped mass matrix case this limit is much smaller. However the overall accuracy is also governed by the numerical elimination (damping) of unresolved modes and the use of the lumped mass matrix can be quite effective.

In this paper we focused on the errors seen when using the trapezoidal rule, Newmark method, and the Bathe time integration schemes with simple linear and bilinear spatial discretizations and uniform meshes with nodes equally spaced. The results are of general value and, also, such spatial discretizations are used in the interior of the analysis geometry when employing AMORE.

A valuable further endeavor is to study the solution errors when using the time integration schemes (with their parameters) in distorted meshes. These more general cases are best studied together with the use of enhanced spatial discretizations, in particular 'overlapping finite elements' that are distortion-insensitive [47–49] and AMORE, and should also consider multiple waves traveling through the mesh.

Furthermore, studies on comparing implicit and explicit time integration schemes in accuracy and computational effort used for wave propagation problems would be of value. Here too the use of overlapping finite elements might be explored.

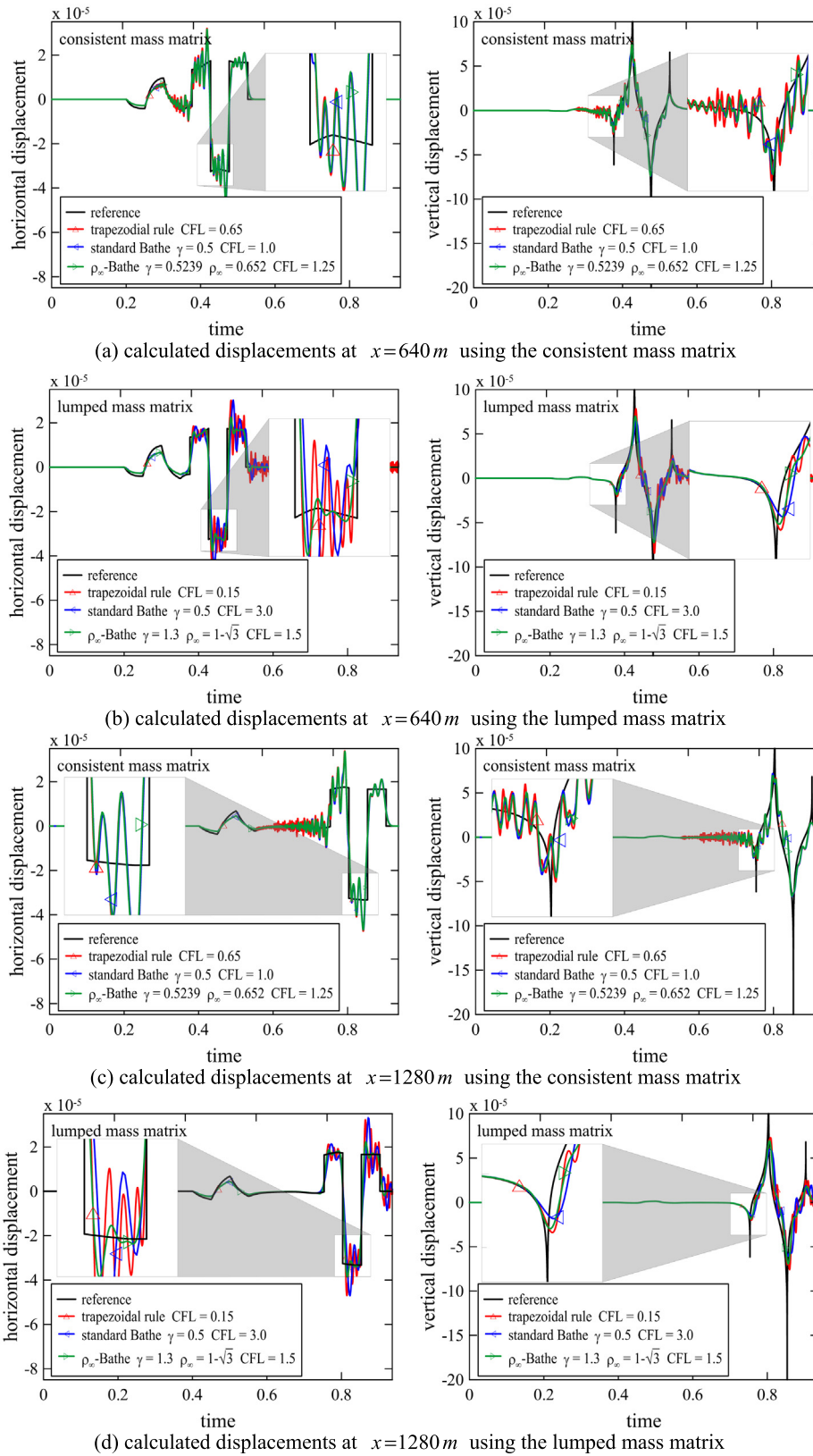


Fig. 30. Time history of horizontal displacements (left) and vertical displacements (right) with the regular mesh ($h = 2$ m) using various Bathe methods and trapezoidal rule when the step functions line load is applied.

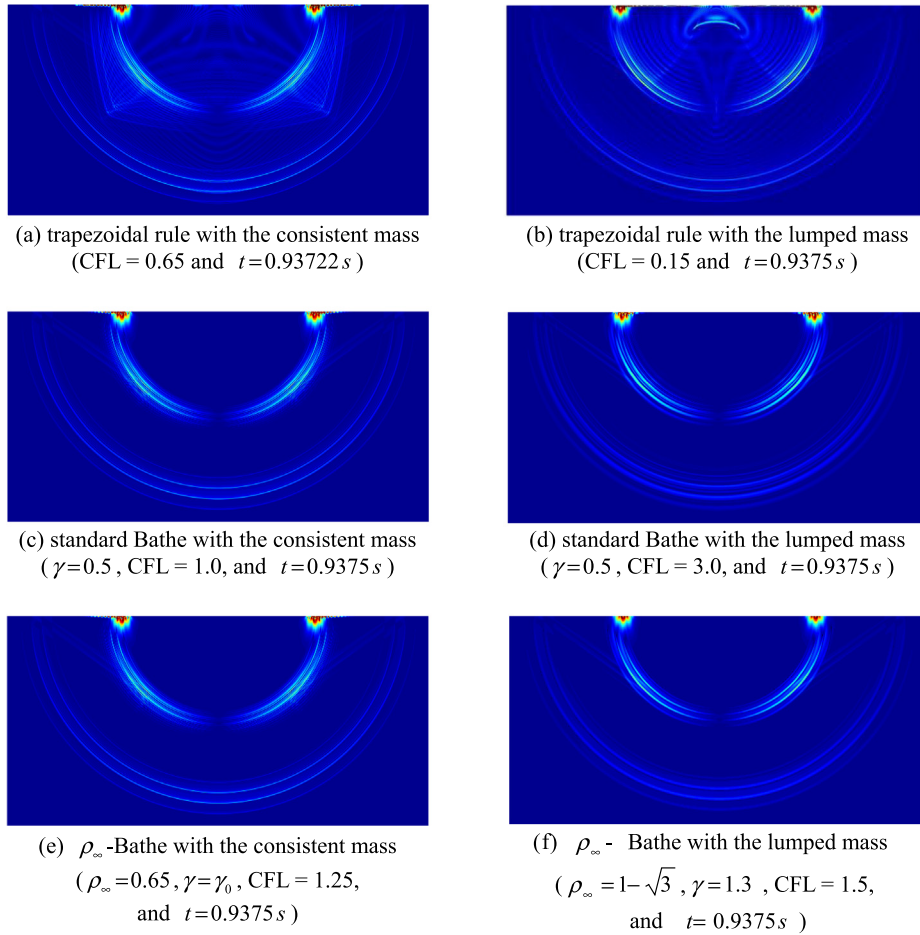


Fig. 31. Snapshot of von Mises stress using various Bathe methods and trapezoidal rule with the consistent mass matrix (left) and lumped mass matrix (right) when the step functions line load is applied.

Declaration of Competing Interest

The authors declared that there is no conflict of interest.

Acknowledgment

This work was partly supported by the Basic Science Research Program (Grant No. 2018R1D1A1B07045805) through the National Research Foundation of Korea (NRF) funded by the Ministry of Education.

Appendix A. Stability conditions for the β_1/β_2 -Bathe scheme with $\beta_2 = 2\beta_1$

In the β_1/β_2 -Bathe method with $\beta_2 = 2\beta_1$, we obtain $\rho(\mathbf{A})|_{\Omega_0=0} = 1$ and $\rho'(\mathbf{A})|_{\Omega_0=0} = 0$, where $\rho'(\mathbf{A})$ is the derivative of $\rho(\mathbf{A})$ with respect to Ω_0 :

$$\rho'(\mathbf{A}) = \frac{\Omega_0}{\rho(\mathbf{A})} \times \frac{(n_2 d_1 - n_1 d_2) \Omega_0^4 - 2(n_0 d_2 - n_2 d_0) \Omega_0^2 + (n_1 d_0 - n_0 d_1)}{(d_2 \Omega_0^4 + d_1 \Omega_0^2 + d_0)^2} \tag{B1}$$

where

$$n_2 = \gamma^2 (s_0 - s_1)(q_0 - q_1); n_1 = \gamma^2 - 4(q_1 + s_1)\gamma + 4(s_0 + s_1)(q_0 + q_1); n_0 = 4; \tag{B2}$$

$$d_2 = q_2 s_2 \gamma^2; d_1 = \gamma^2 + 4q_2 s_2; \text{ and } d_0 = 4$$

Also, the number of roots of the equation $\rho'(\mathbf{A}) = 0$ for $\Omega_0 \geq 0$ is less than or equal to two except when $\gamma = 1$ with $\beta_1 = 0.5$ and $\gamma = 0$ with $\beta_1 = 0.25$. With $\gamma = 1$ and $\beta_1 = 0.5$, and $\gamma = 0$ and $\beta_1 = 0.25$, $\rho(\mathbf{A})$ of the β_1/β_2 -Bathe scheme with $\beta_2 = 2\beta_1$ is 1.0 for $\Omega_0 \geq 0$; thus, the scheme is non-dissipative and unconditionally stable. Therefore, the conditions of unconditional stability for the β_1/β_2 -Bathe method with $\beta_2 = 2\beta_1$ are

$$\rho'(\mathbf{A})|_{\Omega_0=\delta} \leq 0 \tag{B3}$$

$$\lim_{\Omega_0 \rightarrow \infty} \rho(\mathbf{A}) \leq 1 \tag{B4}$$

where δ is a positive infinitesimal (thus, $\delta^n \approx 0$ for $n \geq 2$) and

$$\rho'(\mathbf{A})|_{\Omega_0=\delta} = \frac{\delta(n_1 d_0 - n_0 d_1)}{2d_1 d_0 \delta + d_0^2} \tag{B5}$$

$$\lim_{\Omega_0 \rightarrow \infty} \rho(\mathbf{A}) = \left(\frac{(s_0 - s_1)(q_0 - q_1)}{q_2 s_2} \right)^{0.5} \tag{B6}$$

With $s_0 = q_0 = \gamma(1 - \beta_1)$, $s_1 = q_1 = \gamma(3\beta_1 - 1) + 1 - 2\beta_1$, and $s_2 = q_2 = 2(1 - \gamma)\beta_1$, Eqs. (B5) and (B6) can be rewritten as Eqs. (B7) and (B8), respectively:

$$\rho'(\mathbf{A})|_{\Omega_0=\delta} \simeq \frac{\delta((q_0 + q_1 - q_2) - 2q_1\gamma)}{(\gamma^2/2 + 2q_2^2)\delta + 1} \quad (\text{B7})$$

With Eqs. (B3) and (B4), we find the range of γ selected to correspond to the value of $\beta_1 \geq 1/4$ so that the β_1/β_2 -Bathe method with $\beta_2 = 2\beta_1$ is unconditionally stable (see B9), while the β_1/β_2 -Bathe method with $\beta_1 < 1/4$ is unstable for all γ since $\rho'(\mathbf{A})|_{\Omega_0=\delta} > 0$.

$$\begin{aligned} \gamma_{s3} \leq \gamma \leq \gamma_{s1} & \quad \text{for } 1/4 \leq \beta_1 < 1/3 \\ \gamma \leq 0.5 & \quad \text{for } \beta_1 = 1/3 \\ \gamma \leq \gamma_{s1} \text{ or } \gamma \geq \gamma_{s2} & \quad \text{for } 1/3 < \beta_1 < 1/2 \\ \gamma \leq \gamma_{s3} \text{ or } \gamma \geq \gamma_{s4} & \quad \text{for } 1/2 \leq \beta_1 < 1 \\ \gamma \leq \gamma_{s3} & \quad \text{for } \beta_1 = 1 \\ \gamma_{s4} \leq \gamma \leq \gamma_{s3} & \quad \text{for } 1 < \beta_1 \end{aligned} \quad (\text{B9})$$

where γ_{s1} and γ_{s2} are roots of the equation $\rho'(\mathbf{A})|_{\Omega_0=\delta} = 0$, and γ_{s3} and γ_{s4} are roots of the equation $\lim_{\Omega_0 \rightarrow \infty} \rho(\mathbf{A}) = 1$:

$$\begin{aligned} \gamma_{s1} &= \frac{4\beta_1 - 1 - \sqrt{(4\beta_1 - 1)(1 - 2\beta_1)}}{6\beta_1 - 2}; \gamma_{s2} = \frac{4\beta_1 - 1 + \sqrt{(4\beta_1 - 1)(1 - 2\beta_1)}}{6\beta_1 - 2}; \\ \gamma_{s3} &= \frac{4\beta_1 - 1}{6\beta_1 - 2}; \text{ and } \gamma_{s4} = -\frac{1}{2\beta_1 - 2} \end{aligned} \quad (\text{B10})$$

References

- [1] Bathe KJ. The finite element method. In: Linderberg T, Wah B, editors. Encyclopedia of computer science and engineering. Hoboken (New Jersey): J. Wiley and Sons; 2009. p. 1253–64.
- [2] Bathe KJ. Frontiers in finite element procedures & applications. In: Topping BHV, Iványi P, editors. Chapter 1 in computational methods for engineering technology. Stirlingshire (Scotland): Saxe-Coburg Publications; 2014.
- [3] Bathe KJ. Finite element procedures. 2nd ed. Watertown (MA): Higher Education Press China; 2016. , <http://meche.mit.edu/people/faculty/kjb@mit.edu>.
- [4] Newmark NM. A method of computation for structural dynamics. J Eng Mech Div (ASCE) 1959;85:67–94.
- [5] Bathe KJ, Wilson EL. Stability and accuracy analysis of direct integration methods. Int J Earthquake Eng Struct Dyn 1973;1:283–91.
- [6] Hilber HM, Hughes TJR, Taylor RL. Improved numerical dissipation for time integration algorithms in structural dynamics. Earthquake Eng Struct Dyn 1977;5:283–92.
- [7] Wood WL, Bossak M, Zienkiewicz OC. An alpha modification of Newmark's method. Int J Numer Meth Eng 1980;15:1562–6.
- [8] Shao HP, Cai CW. The direct integration three-parameters optimal schemes for structural dynamics. In: Proceedings of the international conference: machine dynamics and engineering applications. Xi'an Jiaotong University Press; 1988. p. C16–20.
- [9] Subbaraj K, Dokainish MA. A survey of direct time-integration methods in computational structural dynamics—II. Implicit methods. Comput Struct 1989;32:1387–401.
- [10] Chung J, Hulbert GM. A time integration algorithm for structural dynamics with improved numerical dissipation: the generalized-alpha method. J Appl Mech (ASME) 1993;60:371–5.
- [11] Tamma KK, Zhou X, Sha D. The time dimension: a theory towards the evolution, classification, characterization and design of computational algorithms for transient/dynamic applications. Arch Comput Methods Eng 2000;7:67–290.
- [12] Tamma KK, Sha D, Zhou X. Time discretized operators. Part 1: Towards the theoretical design of a new generation of a generalized family of unconditionally stable implicit and explicit representations of arbitrary order for computational dynamics. Comput Methods Appl Mech Eng 2003;192:257–90.
- [13] Sha D, Zhou X, Tamma KK. Time discretized operators. Part 2: Towards the theoretical design of a new generation of a generalized family of unconditionally stable implicit and explicit representations of arbitrary order for computational dynamics. Comput Methods Appl Mech Eng 2003;192:291–329.
- [14] Zhou X, Tamma KK. Design, analysis, and synthesis of generalized single step single solve and optimal algorithms for structural dynamics. Int J Numer Meth Eng 2004;59:597–668.
- [15] Chang SY. Dissipative, noniterative integration algorithms with unconditional stability for mildly nonlinear structural dynamic problems. Nonlinear Dyn 2015;79(2):1625–49.
- [16] Malakieh MM, Shojaee S, Javaran SH. Development of a direct time integration method based on Bezier curve and 5th-order Bernstein basis function. Comput Struct 2018;194:15–31.
- [17] Dong S. BDF-like methods for nonlinear dynamic analysis. J Comput Phys 2010;229(8):3019–45.
- [18] Chandra Y, Zhou Y, Stanculescu I, Eason T, Spottswood S. A robust composite time integration scheme for snap-through problems. Comput Mech 2015;55(5):1041–56.
- [19] Wen WB, Wei K, Lei HS, Duan SY, Fang DN. A novel sub-step composite implicit time integration scheme for structural dynamics. Comput Struct 2017;182:176–86.
- [20] Wen W, Tao Y, Duan S, Yan J, Wei K, Fang D. A comparative study of three composite implicit schemes on structural dynamic and wave propagation analysis. Comput Struct 2017;190:126–49.
- [21] Huang C, Fu M. A composite collocation method with low-period elongation for structural dynamics problems. Comput Struct 2018;195:74–84.
- [22] Kim W, Choi SY. An improved implicit time integration algorithm: The generalized composite time integration algorithm. Comput Struct 2018;196:341–54.
- [23] Zhang HM, Xing YF. Optimization of a class of composite method for structural dynamics. Comput Struct 2018;202:60–73.
- [24] Li J, Yu K. An alternative to the Bathe algorithm. Appl. Math. Model. 2019;69:255–72.
- [25] Bathe KJ, Baig MMI. On a composite implicit time integration procedure for nonlinear dynamics. Comput Struct 2005;83:2513–4.
- [26] Bathe KJ. Conserving energy and momentum in nonlinear dynamics: a simple implicit time integration scheme. Comput Struct 2007;85:437–45.
- [27] Bathe KJ, Noh G. Insight into an implicit time integration scheme for structural dynamics. Comput Struct 2012;98–99:1–6.
- [28] Zhang J, Liu Y, Liu D. Accuracy of a composite implicit time integration scheme for structural dynamics. Int J Numer Meth Eng 2017;109:368–406.
- [29] Noh G, Bathe KJ. Further insights into an implicit time integration scheme for structural dynamics. Comput Struct 2018;202:15–24.
- [30] Noh G, Bathe KJ. An explicit time integration scheme for the analysis of wave propagations. Comput Struct 2013;129:178–93.
- [31] Soares D. A novel family of explicit time marching techniques for structural dynamics and wave propagation models. Comput Methods Appl Mech Eng 2016;311:838–55.
- [32] Kwon S-B, Lee J-M. A non-oscillatory time integration method for numerical simulation of stress wave propagations. Comput Struct 2017;192:248–68.
- [33] Kim W, Lee JH. An improved explicit time integration method for linear and nonlinear structural dynamics. Comput Struct 2018;206:42–53.
- [34] Noh G, Bathe KJ. The Bathe time integration method with controllable spectral radius: the ρ_∞ -Bathe method. Comput Struct 2019;212:299–310.
- [35] Malakieh MM, Shojaee S, Bathe KJ. The Bathe time integration method revisited for prescribing desired numerical dissipation. Comput Struct 2019;212:289–98.
- [36] Noh G, Bathe KJ. For direct time integrations: a comparison of the Newmark and ρ_∞ -Bathe schemes. Comput Struct 2019;225:1–12.
- [37] Krieg RD, Key SW. Transient shell response by numerical time integration. Int J Numer Meth Eng 1973;7(3):273–86.
- [38] Mullen R, Belytschko T. Dispersion analysis of finite element semidiscretizations of the two-dimensional wave equation. Int J Numer Meth Eng 1982;18(1):11–29.
- [39] Marfurt KJ. Accuracy of finite-difference and finite-element modeling of the scalar and elastic wave equations. Geophysics 1984;49(5):533–49.
- [40] Babuška I, Ihlenburg F, Paik ET, Sauter SA. A generalized finite element method for solving the Helmholtz equation in two dimensions with minimal pollution. Comput Methods Appl Mech Eng 1995;128(3–4):325–59.
- [41] Christon MA. The influence of the mass matrix on the dispersive nature of the semi-discrete, second-order wave equation. Comput Methods Appl Mech Eng 1999;173(1–2):147–66.
- [42] Guddati MN, Yue B. Modified integration rules for reducing dispersion error in finite element methods. Comput Methods Appl Mech Eng 2004;193(3–5):275–87.
- [43] Idesman AV, Schmidt M, Foley JR. Accurate finite element modeling of linear elastodynamics problems with the reduced dispersion error. Comput Mech 2011;47(5):555–72.
- [44] Ham S, Bathe KJ. A finite element method enriched for wave propagation problems. Comput Struct 2012;94:1–12.
- [45] Noh G, Ham S, Bathe KJ. Performance of an implicit time integration scheme in the analysis of wave propagations. Comput Struct 2013;123:93–105.
- [46] Kim KT, Bathe KJ. Transient implicit wave propagation dynamics with the method of finite spheres. Comput Struct 2016;173:50–60.
- [47] Kim KT, Zhang L, Bathe KJ. Transient implicit wave propagation dynamics with overlapping finite elements. Comput Struct 2018;199:18–33.
- [48] Bathe KJ. The AMORE paradigm for finite element analysis. Adv Eng Softw 2019;130:1–13.
- [49] Huang J, Bathe KJ. Quadrilateral overlapping elements and their use in the AMORE paradigm. Comput Struct 2019;222:25–35.